Influence of inerter-based damper installations on control efficiency of building structures

First published: **06 Jan 2022**

which has been published in final form at

https://onlinelibrary.wiley.com/journal/15452263

Influence of inerter-based damper installations on control efficiency of building structures

Tiancheng Xu[1], Gang Yang[1], Yancheng Li[2] and Tao Lai[1]

1 College of Civil Engineering, Nanjing Tech University, Nanjing 211816, China

2 School of Civil and Environmental Engineering, University of Technology Sydney, Ultimo, NSW 2007, Australia

Corresponding email: yli@njtech.edu.cn

Abstract:

In this study, the influences of the installation position of inerter-based dampers (IBDs) on each modal response, IBDs stroke, inerter stroke, and control force produced by IBDs are derived analytically. A new installation scheme to implement the two ends of the IBDs across multiple storeys, i.e., span-storey installation, is proposed to enhance the control performance of IBDs. The paper starts with a single degrees of freedom (SDOF) system with IBD and optimal parameters formulas of IBD based on H_2 criterion are obtained. Then the multiple degrees of freedom (MDOF) system with the span-storey installed IBD is analyzed and an optimization design method is proposed for the new installation method. The proposed design method of span-storey installed IBDs can reuse the design formulas in SDOF case and can reduce response of target modal. A 3-storey benchmark building model is selected as case study and the results reveal that IBDs with new installation method outperform tuned mass damper (TMD) and the span-storey installation of IBDs is beneficial for control of first modal. Also, the proposed method is validated by the sensitivity analysis and impulse response analysis in case study. Besides, through the comparison of span-storey mounting strategy and increasing inertance strategy, one finds that the span-storey installation of IBDs can substantially improve the efficiency of inerter and damper and reduce the control force by amplifying the drift. Through the simulation on a 9-storey nonlinear benchmark building, the span-storey installed IBDs are found to possess high efficiency in seismic control and can significant reduce the building damage during earthquake.

Author keywords: Inerter-based damper; structural control; span-storey installation; MDOF structures; optimal design;

1. Introduction

In recent years, inerter has been introduced into structural control as an effective passive control device. Inerter, invented by Smith [1], is a two-terminal mechanical element, and the force of two terminals of inerter is $F=b\ddot{y}_{int}$, where $\ddot{y}_{int}$ is the relative acceleration between the two terminals of inerter. The proportional coefficient *b* is called inertance or apparent mass with the same unit as mass. The distinguished advantage of inerter is that the inertance can be hundreds of times higher than the actual mass through the rack or ball-screw mechanisms. Therefore, inerter can achieve excellent vibration control performance with low mass cost and this make it an attractive device for structural control.

Up to date, considerable efforts have been devoted to study the ability of IBDs in mitigation of seismic and wind responses in civil engineering structures. Ikago et al. [2] proposed a tuned viscous mass damper (TVMD) containing inerter for seismic control of buildings. Then a small-scale TVMD with inerter realized by ball-screw mechanism was manufactured and the control effect was verified by shaking table tests [3]. Tuned mass damper inerter (TMDI), proposed by Marian et al. in 2014 [4], is another promising structural control device and the optimal design problem of TMDI was explored by Pietrosanti et al. [5]. In addition, there are many studies using TMDI to enhance the base isolation systems [6][7][8][9] and reduce the vibration of bridge [10]. Tuned inerter damper (TID) is another

inerter-based passive control device proposed by Lazar et al. [11] for seismic control of MDOF structure as a potential alternative to TMD. The configuration of TID is similar to that of TMD, i.e. an inerter in-series connected to a parallel configured spring and dashpot. However, the main difference is that TID operates on the relative motion at the two terminals while TMD operates on the absolute motion. TID has been attracting considerable interest because it has great vibration control performance with small mass and compact configuration. A number of literatures [12][13][14][15] have investigated the efficiency of TID for vibration control of cables. Hu et al. [16][17] investigated the optimal design and evaluated the performances of various inerter-based dynamic vibration absorbers and isolators including the TID and TVMD. Wen et al. [18] studied the parameters and location optimizations of multiple TIDs and TVMDs for seismic control of MDOF structures and the numerical simulation verified the validity in suppressing responses of multiple modes. From recent researches of TID, they mainly focus on novel optimization design [19] [20] [21], reliability under various loads [22][23], and the role of damping in TID [24][25].

As conventional two terminals passive control devices, damping mechanism can improve the ability of energy dissipation by installing the damper between two points where a significant displacement difference is expected. Aly [26] applied outer bracing and lever mechanism to connect magneto-rheological dampers between ground and a specific storey for better energy dissipation in high-rise buildings subjected to wind loads. Utilizing toggle-brace mechanisms, Constantinou et al. [27] developed three drift magnification mechanisms to magnify the displacements and effect of damping devices. In this respect, as new two terminals devices, inerter and various IBDs devices can also utilize above displacement magnification concept to achieve an excellent vibration control performance. However, only limited studies have focused on the promising method. Hwang et al. [28] utilized a toggle brace mechanism to improve the performance of inerter, especially in structures with small drift. The span-storey installation scheme, i.e., IBD spans more than one storey between the two terminals, is first employed by Giaralis and Petrini in 2017 [29] to improve the performance of TMDI in wind-induced vibration control. In [30], Giaralis and Taflanidis used the span-storey TMDI to mitigate the seismic responses of buildings. The numerical results show that span-storey installation can enhance the performance and robustness of TMDI. In above research [29-30], the idea of span storey installation is used as an example but not fully investigated. Recently, Xue et al. [31] proposed a cable-bracing inerter system (CBIS) in which a TVMD is span-storey installed on MDOF structure by a cable-bracing device. Meanwhile, a numerical design procedure of CBIS is developed and the seismic control effect is explored. To sum up, there are few studies considered TMDI and TVMD devices to be implemented using span-storey installation. However, the fundamental mechanism and analytical design method of the storey installation are not addressed. For example, the fundamental understandings on the effect of installation strategy on structural or control device responses and the choice of optima installation location for span-storey installed IBDs is to be explored. The vibration control performance of the span-storey installed IBDs is yet to be evaluated through response analysis or comparing with TMD or non-span-storey installed IBDs. In practical design, a simple analytical design method is effective for vibration control and is of interest and significance for applications. However, to the best of the authors' knowledge, the analytical design or closed-form solutions for span-storey installed IBDs have not been reported in literatures. This paper presents a theoretical study on the span-storey installation of IBDs. The analytical optimal design of two typical IBDs are examined and the evaluation of their performances are conducted on benchmark building. A theoretical model is introduced for MDOF structure controlled by span-storey installed IBD or TMD device. The influences of installation location on the modal response, the IBDs stroke, the inerter stroke, and the control force produced by IBDs are investigated. In addition, a simple design method is proposed for both IBDs and TMD. A 3-storey benchmark building model is used to illustrate the proposed method and then sensitivity analysis and impulse response analysis are carried out to verify the method. A comparison between increasing inertance and span-storey installation is designed to evaluate the enhance effect of span-storey scheme. Finally, a seismically

excited 9-storey nonlinear benchmark building is used to investigate the effectiveness of seismic control for span-storey installed IBDs.

2. Single DOF Structure Installed IBDs

Figure 1 (a) shows a SDOF ground excited structure with a two-node IBDs installed between ground and structure or a tuned mass damper (TMD) attached to structure. Here the control performance is represented generically by a transfer function $D(s)$, where *s* is the Laplace variable, regardless the control device used. In this paper two types of IBDs named IBD-I and IBD-II, as shown in Figure 1 (b) and (c), are discussed. IBD-I is actually the TID since the configuration is an inerter in-series connected to a parallel connection of spring and dashpot. While in IBD-II, an inerter, a spring and a dashpot is configured in series. In addition, a TMD as shown in Figure 1 (d) is also investigated for comparison. In Figure 1, m_s, c_s, and k_s are mass, damping, and stiffness of primary structure, respectively. b is the inertance of inerter in IBDs and m_d is the secondary mass of TMD. The c_d and k_d are the damping and stiffness coefficients of IBDs or TMD, respectively. $A_g = L(a_g)$ denotes the Laplace transform of ground acceleration and the operator $\mathrm{L}(\cdot)$ denotes Laplace transform. $Y_s = \mathrm{L}(y_s)$ denotes the displacement of primary mass relative to ground. $Y_{int} = \mathrm{L}(y_{int})$ denotes the relative displacement between the two terminals of inerter and $Y_{\mathrm{IBD}} = \mathrm{L}(y_{\mathrm{IBD}})$ denotes the relative displacement between the two terminals of IBDs. Note in this case there has $Y_{\mathrm{IBD}} = Y_s$. F_p denotes the control force produced by the control devices acting at the storey below (here is the ground) and F_p denotes the control force generated by the control devices acting at the upper storey.

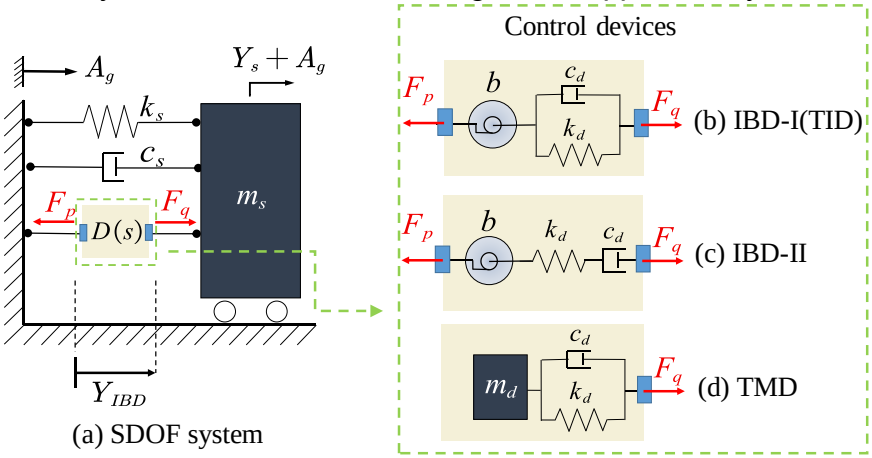

Figure 1 The sketch of the (a) SDOF controlled structure; (b) type-I of IBD; (c) type-II of IBD; (d) TMD.

Considering zero initial conditions, the equation of motions for IBD-I controlled system can be written in Laplace domain as

$$\begin{aligned} m_s s^2 Y_{\mathrm{IBD}} + c_s s Y_{\mathrm{IBD}} + k_s Y_{\mathrm{IBD}} &= -m_s A_g + (c_d s + k_d)(Y_{int} - Y_{\mathrm{IBD}}) \\ b s^2 Y_{int} + (c_d s + k_d)(Y_{int} - Y_{\mathrm{IBD}}) &= 0 \end{aligned} \tag{1}$$

and for IBD-II controlled system yield

$$\begin{aligned} m_s s^2 Y_{\mathrm{IBD}} + c_s s Y_{\mathrm{IBD}} + k_s Y_{\mathrm{IBD}} &= -m_s A_g + \frac{c_d s + k_d}{c_d s k_d}(Y_{int} - Y_{\mathrm{IBD}}) \\ b s^2 Y_{int} + \frac{c_d s + k_d}{c_d s k_d}(Y_{int} - Y_{\mathrm{IBD}}) &= 0 \end{aligned} \tag{2}$$

The control forces generated at both terminals of IBDs are equal in magnitude with opposite directions. The control forces for IBD-I are

$$\begin{cases} F_p = -bs^2 Y_{int} \\ F_q = (c_d s + k_d)(Y_{int} - Y_{\mathrm{IBD}}) \end{cases} \tag{3}$$

and for IBD-II the equations are

$$\begin{cases} F_p = -bs^2 Y_{int} \\ F_q = \dfrac{c_d s + k_d}{c_d s k_d}(Y_{int} - Y_{\mathrm{IBD}}) \end{cases} \tag{4}$$

In fact, all control forces can be represented generically as $|F_p| = |F_q| = D(s) Y_{\mathrm{IBD}}$. While for TMD, there is only one control force F_q formulated by

$$F_q = D(s)(Y_s + A_g) \tag{5}$$

$D(s)$ represents the transfer function of each device and is given by

$$\begin{cases} D(s) = s \Big/ \left(\dfrac{1}{\frac{k_d}{s} + c_d} + \dfrac{1}{bs}\right) & \text{,for IBD-I} \\ D(s) = s \Big/ \left(\dfrac{1}{bs} + \dfrac{1}{c_d} + \dfrac{s}{k_d}\right) & \text{,for IBD-II} \\ D(s) = s \Big/ \left(\dfrac{1}{\frac{k_d}{s} + c_d} + \dfrac{1}{m_d s}\right) & \text{,for TMD} \end{cases} \tag{6}$$

For IBDs controlled system, the equation of motion can be rewritten as

$$m_s s^2 Y_{\mathrm{IBD}} + c_s s Y_{\mathrm{IBD}} + k_s Y_{\mathrm{IBD}} = -m_s A_g - D(s) Y_{\mathrm{IBD}} \tag{7}$$

The transfer function from A_g to Y_{IBD} is

$$H(s) = \frac{Y_{\mathrm{IBD}}}{A_g} = \frac{-m_s}{m_s s^2 + c_s s + k_s + D(s)} \tag{8}$$

For passive control device, selection of system parameters is one of the most important aspects. To this end, several dimensionless parameters are introduced as

$$\mu = \begin{cases} \dfrac{b}{m_s}, & \text{for TID} \\ \dfrac{m_d}{m_s}, & \text{for TMD} \end{cases}, \quad \gamma = \frac{\omega_d}{\omega_s}, \quad \xi_d = \begin{cases} \dfrac{c_d}{2b\omega_d}, & \text{for TID} \\ \dfrac{c_d}{2m_d\omega_d}, & \text{for TMD} \end{cases} \tag{9}$$

Where μ denotes inertance-to-mass ratio (for IBDs) or mass ratio (for TMD); ω_d is natural frequency of TID $\omega_d = \sqrt{k_d / b}$ or TMD ($\omega_d = \sqrt{k_d / m_d}$)and $\omega_s = \sqrt{k_s / m_s}$ is natural frequency of primary structure; γ denotes tuning ratio and ξ_d denotes damping ratio. One of the most important aspect in passive control device design is the choice of optimization parameters. In this case the target of optimization design is to find optimal γ and ξ_d to minimize the performance index with given μ. Here the H_2 optimization is used and the ground motion excitation is considered as ideal white noise. The performance index is the area of frequency response curve which is defined as follows [32]

$$J = \frac{E[y_s^2]}{2\pi S_0 \omega_s} \tag{10}$$

where $E\left[y_s^2\right]$ is the mean square value of the displacement of the primary structure and S_0 is the uniform power spectrum density function. $E\left[y_s^2\right]$ is calculated as

$$E[y_s^2]=S_0\omega_s\int_{-\infty}^{+\infty}|H(\lambda)|^2\mathrm{d}\lambda \tag{11}$$

Substituting Eq. (11) into (10), one obtains

$$J=\frac{1}{2\pi}\int_{-\infty}^{+\infty}|H(\lambda)|^2\mathrm{d}\lambda \tag{12}$$

According to Eq. (12), the performance index is the non-dimensional mean square response of the system subjected to ideal white noise excitation.

The explicit analytical solutions of the design parameters can be obtained when primary structure is undamped. Considering $c_s=0$, the optimal parameters of IBDs are derived in Appendix A according to Eq. (8). While for TMD, the optimal parameters can be found in [33]. All the optimal parameters are listed in Table 1.

Table 1 The optimal parameters of control devices

Type of control devices	Tuning ratio γ	Damping ratio ξ_d	Performance index J
IBD-I	$\frac{\sqrt{2(\mu+2)}}{2(\mu+1)}$	$\sqrt{\frac{\mu(4+3\mu)}{8(1+\mu)(2+\mu)}}$	$\sqrt{\frac{4+3\mu}{4\mu(\mu+1)}}$
IBD-II	1	$\frac{1}{2\sqrt{\mu}}$	$\frac{1}{\sqrt{\mu}}$
TMD	$\frac{\sqrt{1-\mu/2}}{1+\mu}$	$\sqrt{\frac{\mu(1-\mu/4)}{4(1+\mu)(1-\mu/2)}}$	$\sqrt{\frac{(1+\mu)^3(1-\mu/4)}{\mu}}$

The variation of all three performance indices against μ is plotted in Figure 2. Overall, it can be seen that the IBD-I has the best performance and the TMD has the worst performance. The performances of IBD-I and IBD-II are rather close. There is a point (μ=0.1) below which three systems have similar performance. When μ is greater than 0.1, the performance of TMD gradually diverges from the other two and gets worse after μ is greater than 0.5. This indicate that for control of relative displacement of SDOF structures, IBDs outperform TMD particularly when μ is larger.

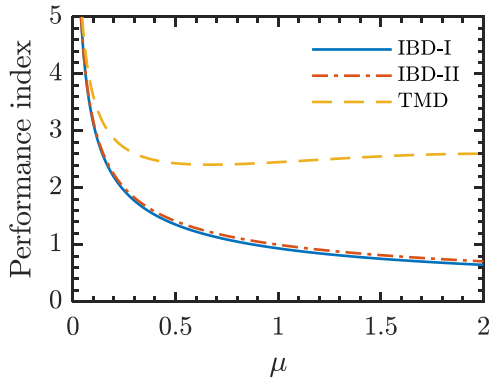

Figure 2 The performance indices of three control devices

3. Multiple DOF Structure installed IBDs

3.1 Equations of motion

A *n*-DOF building model with a IBD system installed between storey p and q is shown in Figure 3. A simple and effective method to realize the span-story installation of IBDs is proposed and illustrated in Figure 3. This method use chevron brace configuration to transmit the relative motion between storey p and q to the two terminals of IBD. For convenience, $L_{p,q}$ is defined as position indicator to identify the installation location of IBDs. The $p \in [0:n-1]$ and $q \in [1:n]$ represents the installation storeys of lower and upper terminals of IBD, respectively. Note q must be greater than p and when *p* = 0 it represents the lower terminal of IBD is connected to the ground. Where m_i and k_i are the lumped mass, and lateral stiffness of i^{th} storey respectively; y_i is the displacement of the i^{th} storey relative to the ground and a_g is the ground acceleration excitation.

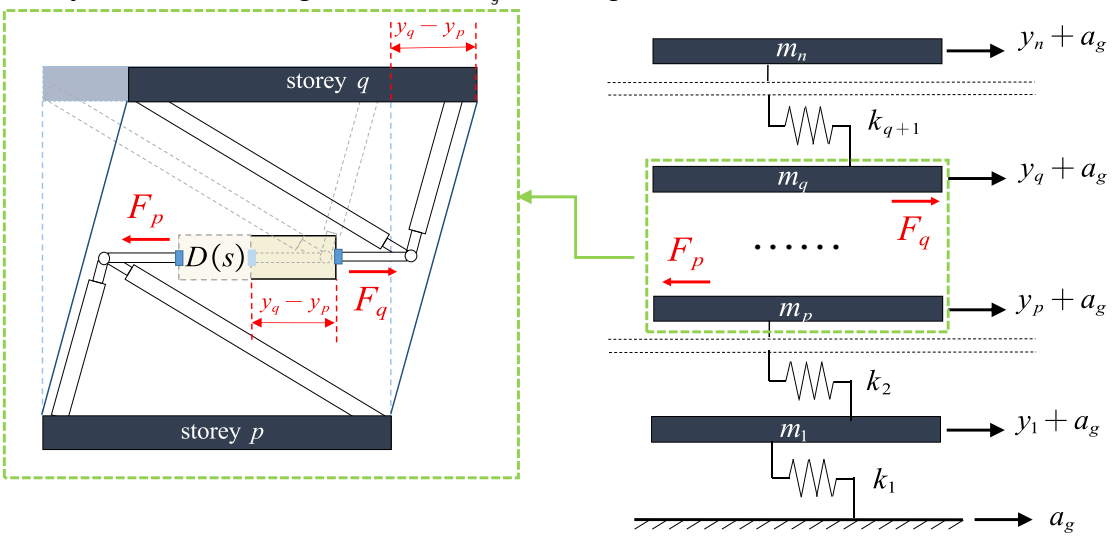

Figure 3. The MDOF structure controlled by a span-storey installed IBD;

Considering zero initial conditions, the equation of motion of the controlled system shown in Figure 3 can be written in Laplace domain as follows

$$\begin{cases} m_1 s^2 Y_1 + k_1 Y_1 + k_2 (Y_1 - Y_2) = -m_1 A_g \\ \vdots \\ m_p s^2 Y_p + k_p (Y_p - Y_{p-1}) + k_{p+1} (Y_p - Y_{p+1}) = -m_p A_g + F_p \\ \vdots \\ m_q s^2 Y_q + k_q (Y_q - Y_{q-1}) + k_{q+1} (Y_q - Y_{q+1}) = -m_q A_g + F_q \\ \vdots \\ m_n s^2 Y_n + k_n (Y_n - Y_{n-1}) = -m_n A_g \\ \mathcal{F}_{\mathrm{IBD}} = 0 \end{cases} \tag{13}$$

where $\mathcal{F}_{\mathrm{IBD}}$ is the equation of motion of IBDs subsystem. Note that in the MDOF system case there has $Y_{\mathrm{IBD}} = Y_q - Y_p$. For IBD-I, the control forces and $\mathcal{F}_{\mathrm{IBD}}$ are

$$\begin{aligned} F_p &= -b s^2 Y_{\mathrm{int}} \\ F_q &= (c_d s + k_d)(Y_{int} - Y_{\mathrm{IBD}}) \\ \mathcal{F}_{\mathrm{IBD}} &= b s^2 Y_{int} + (c_d s + k_d)(Y_{int} - Y_{\mathrm{IBD}}) \end{aligned} \tag{14}$$

While for IBD-II, the control forces are

$$
\begin{aligned}
F_p &= -bs^2 Y_{int} \\
F_q &= \frac{c_d s + k_d}{c_d s k_d}(Y_{int} - Y_{\mathrm{IBD}}) \\
\mathscr{F}_{\mathrm{IBD}} &= bs^2 Y_{int} + \frac{c_d s + k_d}{c_d s k_d}(Y_{int} - Y_{\mathrm{IBD}})
\end{aligned}
\tag{15}
$$

The first *n* equations of Eq. (13) can be rewritten as matrix form, that is

$$
[\mathrm{M}]s^2\{\mathrm{Y}\}+[\mathrm{K}]\{\mathrm{Y}\}=-[\mathrm{M}]\{I_n\}A_g+\begin{pmatrix}\vdots\\ F_p\\ \vdots\\ F_q\\ \vdots\end{pmatrix} \tag{16}
$$

where

$$
[\mathrm{M}]=\begin{bmatrix} m_1 & 0 & \cdots & 0\\ 0 & m_2 & \cdots & 0\\ \vdots & \vdots & \ddots & \vdots\\ 0 & 0 & \cdots & m_n\end{bmatrix},[\mathrm{K}]=\begin{bmatrix} k_1+k_2 & -k_2 & 0 & \cdots & 0\\ -k_2 & k_2+k_3 & -k_3 & \cdots & 0\\ 0 & -k_3 & k_3+k_4 & \cdots & \vdots\\ \vdots & \vdots & \vdots & \ddots & -k_n\\ 0 & 0 & \cdots & -k_n & k_n\end{bmatrix},\{\mathrm{Y}\}=\begin{pmatrix}Y_1\\ Y_2\\ \vdots\\ Y_3\end{pmatrix},\{I_n\}=\begin{pmatrix}1\\ 1\\ \vdots\\ 1\\ 1\end{pmatrix} \tag{17}
$$

In this application, the structural damping are considered as Rayleigh damping with the form $[\mathrm{C}]=\alpha_0[\mathrm{M}]+\alpha_1[\mathrm{K}]$, where α_0 and α_1 are the damping coefficients.

Besides, the transfer function form A_g to Y_i is denoted as $H_i(s)$ and can be obtained from Eq. (13).

3.2 The equivalent SDOF system

The core concept of the design approach is to express Eq. (13) in a form similar to the SDOF case by transforming the original matrix equation to scalar modal equations. Based on the fact that the control forces produced by IBDs are equal and opposite, here the magnitude of F_q is substituted with $|F_p|$, i.e., $|bs^2Y_{int}|$, regardless the IBD-I or IBD-II is considered. Considering structural damping $[\mathrm{C}]$, the Eq. (16) can be rewritten as

$$
[\mathrm{M}]s^2\{\mathrm{Y}\}+[\mathrm{C}]s\{\mathrm{Y}\}+[\mathrm{K}]\{\mathrm{Y}\}=-[\mathrm{M}]\{I_n\}A_g+\begin{pmatrix}\vdots\\ bs^2Y_{int}\\ \vdots\\ -bs^2Y_{int}\\ \vdots\end{pmatrix} \tag{18}
$$

To explore the influence of span-storey installation on different modal responses, modal analysis is carried out here. The modal matrix $[\Phi]$ and coordinates $\{Q\}$ are defined as,

$$
[\Phi]=[\{\phi_1\},\{\phi_2\},\ldots,\{\phi_n\}]=\begin{bmatrix}\phi_{1,1} & \phi_{1,2} & \cdots & \phi_{1,n}\\ \phi_{2,1} & \phi_{2,2} & \cdots & \phi_{2,n}\\ \vdots & \vdots & \ddots & \vdots\\ \phi_{n,1} & \phi_{n,2} & \cdots & \phi_{n,n}\end{bmatrix},\{Q\}=\begin{pmatrix}q_1\\ q_2\\ \vdots\\ q_n\end{pmatrix} \tag{19}
$$

Since $[\mathrm{C}]$ is an orthogonal damping matrix, the modal mass, damping, and stiffness terms are defined as

$$
m_i^*=\{\phi_i\}^{\mathrm{T}}[\mathrm{M}]\{\phi_i\},\ c_i^*=\{\phi_i\}^{\mathrm{T}}[\mathrm{C}]\{\phi_i\},\ k_i^*=\{\phi_i\}^{\mathrm{T}}[\mathrm{K}]\{\phi_i\}=\omega_i^2 m_i^* \tag{20}
$$

where superscript T denotes matrix transpose and ω_i denotes the i^{th} natural frequency of undamped primary structure. The responses of primary structure $\{\mathrm{Y}\}$ can be represented in terms of modal vectors and coordinates

$$\begin{pmatrix} Y_1 \\ Y_2 \\ \vdots \\ Y_n \end{pmatrix} = [\Phi]\{Q\} = \{\phi_1\}q_1 + \{\phi_2\}q_2 + \cdots + \{\phi_n\}q_n \tag{21}$$

Using this transformation and pre-multiplying both side by $[\Phi]^{\mathrm{T}}$, the Eq. (18) can be reduced to a set of equations for $\{q_1, q_2, \ldots q_n\}$ and each has the form as

$$m_i^* q_i s^2 + c_i^* q_i s + k_i^* q_i = -\{\phi_i\}^{\mathrm{T}}[\mathrm{M}]\{I_n\}A_g - (\phi_{q,i} - \phi_{p,i})bs^2 Y_{int} \tag{22}$$

where $i \in [1, 2, \cdots, n]$. In general, $\{\mathrm{Y}\}$ is obtained by superposing all the generalized coordinates, i.e. $\{\mathrm{Y}\} = \{\phi_1\}q_1 + \{\phi_2\}q_2 + \cdots + \{\phi_n\}q_n$. Assuming that only the i^{th} modal response is dominated and there is no significant modal interaction, which leads to $\{Y\} = \{\phi_j\}q_i$. The responses of storey with the IBDs mounted can also be expressed approximately as

$$Y_p \approx \phi_{p,i} \times q_i \text{ and } Y_q \approx \phi_{q,i} \times q_i \tag{23}$$

Furthermore, the coordinate q_i can be solved from Eq. (23), that is

$$q_i = \frac{Y_q - Y_p}{\phi_{q,i} - \phi_{p,i}} = \frac{Y_{\mathrm{IBD}}}{\phi_{q,i} - \phi_{p,i}} \tag{24}$$

After substituting Eq. (24) into Eq. (22) and rearranging the result, one obtains

$$m_{ie}^* Y_{\mathrm{IBD}} s^2 + c_{ie}^* Y_{\mathrm{IBD}} s + k_{ie}^* Y_{\mathrm{IBD}} = -m_{ie}^* \Psi A_g - bs^2 Y_{int} \tag{25}$$

where

$$m_{ie}^* = \frac{m_i^*}{(\phi_{q,i} - \phi_{p,i})^2}, c_{ie}^* = \frac{c_i^*}{(\phi_{q,i} - \phi_{p,i})^2}, k_{ie}^* = \frac{k_i^*}{(\phi_{q,i} - \phi_{p,i})^2}, \ \Psi = (\phi_{q,i} - \phi_{p,i})\frac{\{\phi_i^T\}[\mathrm{M}]\{I_n\}}{m_{ie}^*} \tag{26}$$

These parameters combine the i^{th} modal and the storey where the IBD is installed. Recalling the fact that the control forces produced by IBDs are equal and opposite, the control force $bs^2 Y_{int}$ in Eq. (25)can be substituted with F_q again. Replacing the first *n* equations of Eq. (13) by the Eq. (25), the Eq. (13) can be rewritten for IBD-I as

$$\begin{cases} m_{ie}^* Y_{\mathrm{IBD}} s^2 + c_{ie}^* Y_{\mathrm{IBD}} s + k_{ie}^* Y_{\mathrm{IBD}} = -m_{ie}^* \Psi A_g + (c_d s + k_d)(Y_{int} - Y_{\mathrm{IBD}}) \\ bs^2 Y_{int} + (c_d s + k_d)(Y_{int} - Y_{\mathrm{IBD}}) = 0 \end{cases} \tag{27}$$

and for IBD-II as

$$\begin{cases} m_{ie}^* Y_{\mathrm{IBD}} s^2 + c_{ie}^* Y_{\mathrm{IBD}} s + k_{ie}^* Y_{\mathrm{IBD}} = -m_{ie}^* \Psi A_g + \dfrac{c_d s + k_d}{c_d s k_d}(Y_{int} - Y_{\mathrm{IBD}}) \\ bs^2 Y_{int} + \dfrac{c_d s + k_d}{c_d s k_d}(Y_{int} - Y_{\mathrm{IBD}}) = 0 \end{cases} \tag{28}$$

Eq. (27) and (28) are similar in form to Eq. (1) and (2), respectively. This indicates that the MDOF structure-IBD system in Figure 3 is equivalent to the SDOF structure-IBD system in Figure 1. Consequently, m_{ie}^*, m_{ie}^*, and k_{ie}^* are equivalent structural parameters.

Built on the equivalent SDOF system derived above, when an IBD is installed between storeys *p* and *q* of a MDOF structure, the equivalent inertance-to-mass ratio for i^{th} mode is defined in terms of the equivalent mass m_{ie}^* as

$$\mu_{ie} = \frac{b}{m_{ie}^*} = \frac{b}{m_i^*}(\phi_{p,i} - \phi_{q,i})^2 = \mu_i \theta_{p,q}^{(i)} \tag{29}$$

where b/m_{ie}^* represents the ratio of inertance to i^{th} modal mass, here denote as μ_i. The term $(\phi_{p,i} - \phi_{q,i})^2$ is subsequently regarded as the amplification factor (AF) of μ_i, here denote as $\theta_{p,q}^{(i)}$, and its value depends on the difference between two entries corresponding to the installation placement of IBD in modal shape vector.

Setting $p = 0$ and following the same procedure, one can get similar conclusion for TMD. When a TMD is attached on storey q, the i^{th} modal AF for TMD is $\theta_{0,q}^{(i)} = \phi_{q,i}^2$. This can be confirmed in [34]. Hence, $\theta_{p,q}^{(i)}$ and $L_{p,q}$ can also be used for TMD as long as setting $p = 0$, where $q \in [1:n]$.Here the IBD-I is considered as example in following investigation.

3.3 The effect of installation scheme

Note that in the equivalent equations Eq. (27) and (28), the key parameters $m_{ie}^*, c_{ie}^*, k_{ie}^*$ and Ψ depends mainly on installation placement $L_{p,q}$. The effects of installation scheme on interesting responses, including the IBDs stroke Y_{IBD}, the inerter stroke Y_{int}, the modal response q_i, and the control force produced by IBDs, are investigated by substitute Eq. (26) into Eq. (27) with key parameters as following:

(i) the transfer function between Y_{IBD} and A_g;

$$\frac{Y_{\text{IBD}}}{A_g} = \frac{\{\phi_i\}^{\text{T}}[\text{M}]\{I_n\}}{\dfrac{m_i s^2 + \tilde{c}_i s + k_i}{\phi_{q,i} - \phi_{p,i}} + \dfrac{\phi_{q,i} - \phi_{p,i}}{\dfrac{1}{k_d + c_d s} + \dfrac{1}{bs^2}}} \tag{30}$$

(ii) the transfer function between Y_{int} and A_g;

$$\frac{Y_{int}}{A_g} = \frac{\{\phi_i\}^{\text{T}}[\text{M}]\{I_n\}}{(m_i s^2 + \tilde{c}_i s + k_i)\dfrac{bs^2 + c_d s + k_d}{c_d s + k_d} + bs^2(\phi_{q,i} - \phi_{p,i})} \tag{31}$$

(iii) the transfer function between q_i and A_g can be derived by substitute Eq. (24) into (30);

$$\frac{q_i}{A_g} = \frac{\{\phi_i\}^{\text{T}}[\text{M}]\{I_n\}}{m_i s^2 + \tilde{c}_i s + k_i + \dfrac{(\phi_{q,i} - \phi_{p,i})^2}{\dfrac{1}{k_d + c_d s} + \dfrac{1}{bs^2}}} \tag{32}$$

(iv) the transfer function between control force of IBDs and A_g can be derived by $F_p = -bs^2 Y_{int}$

$$\frac{F}{A_g} = \frac{\{\phi_i\}^{\text{T}}[\text{M}]\{I_n\}bs^2}{(m_i s^2 + \tilde{c}_i s + k_i)\dfrac{bs^2 + c_d s + k_d}{c_d s + k_d} + bs^2(\phi_{q,i} - \phi_{p,i})} \tag{33}$$

Except for optimization of parameters c_d and k_d, the control performance of IBD-I is mainly determined by the value of inertance b and the choice of installation placement $L_{p,q}$. This can be validated in Eq. (32), i.e., a larger value of $\theta_{p,q}^{(i)}$ or b will both reduce the modal response q_i and vice versa. However, the effects of b or $L_{p,q}$ on other responses are difficult to determine. For example in Eq. (30), the influence of installation placement represented by $(\phi_{q,i} - \phi_{p,i})$ on the Y_{IBD}

and the influence of inertance b on the control force F in Eq. (33). In fact, this can be addressed by focusing on the resonance response and ignoring the modal damping. Substituting $s = j\omega_i$ and letting $c_i^* = 0$ in above equations, where $j = \sqrt{-1}$ is the imaginary unit, the magnitude of resonance responses transfer function can be obtained as

$$\begin{aligned}
&\left|\frac{Y_{\mathrm{IBD}}}{A_g}\right| = \frac{\left|\{\phi_i\}^{\mathrm{T}}[\mathrm{M}]\{I_n\}\right|}{\left|\phi_{q,i} - \phi_{p,i}\right|}\left(\sqrt{\frac{1}{k_d^2 + c_d^2\omega_i^2}} + \frac{1}{b\omega_i^2}\right),\ \left|\frac{Y_{int}}{A_g}\right| = \frac{\left|\{\phi_i\}^{\mathrm{T}}[\mathrm{M}]\{I_n\}\right|}{b\omega_i^2\left|\phi_{q,i} - \phi_{p,i}\right|}, \\
&\left|\frac{q_i}{A_g}\right| = \frac{\left|\{\phi_i\}^{\mathrm{T}}[\mathrm{M}]\{I_n\}\right|}{(\phi_{q,i} - \phi_{p,i})^2}\left(\sqrt{\frac{1}{k_d^2 + c_d^2\omega_i^2}} + \frac{1}{b\omega_i^2}\right),\ \left|\frac{F}{A_g}\right| = \frac{\left|\{\phi_i\}^{\mathrm{T}}[\mathrm{M}]\{I_n\}\right|}{\left|\phi_{q,i} - \phi_{p,i}\right|}
\end{aligned} \tag{34}$$

From Eq. (34) it can be seen that the larger the $\left|\phi_{q,i} - \phi_{p,i}\right|$ or inertance b, the better the mitigation in the maximum resonance response of Y_{IBD}, Y_{int}, and q_i, and vice versa. In particular, the maximum control force will decreases as $\left|\phi_{q,i} - \phi_{p,i}\right|$ increases but the variation of inertance b has no influence on maximum control force. Following the same procedure, similar conclusions can be obtained for IBD-II.

3.4 Optimization design

According to section 3.3, the optimal installation placement of IBDs for reducing the modal response q_i can be determined as the $L_{p,q}$ which can maximize the $\theta_{p,q}^{(i)}$. Form section 3.2, it can be inferred that the optimal parameters c_d and k_d of span-storey installed IBDs can be obtained by the optimization method presented in section 2. However, it should be noted that Eq. (27) and (1) or Eq. (28) and (2) are not exactly the same due to the terms Ψ is not 1. Therefore, the influence of the presence of Ψ on parameters optimization needs to be investigated.

Firstly, one can obtain the transfer functions between Y_{IBD} and A_g from Eq. (27)

$$\frac{Y_{\mathrm{IBD}}}{A_g} = \frac{-m_{ie}^*}{m_{ie}^* s^2 + c_{ie}^* s + k_{ie}^* + D(s)}\Psi \tag{35}$$

Here, the right side of Eq. (35) is not exactly identical to that of the Eq. (8) due to the presence of Ψ. In addition, the modal response q_i is more suitable as an optimization target instead of the stroke response Y_{IBD}. Based on this, replacing the Y_{IBD} and Ψ in Eq. (35) according to Eq. (24) and (26), one obtains

$$\frac{q_i}{A_g} = \frac{-m_{ie}^*}{m_{ie}^* s^2 + c_{ie}^* s + k_{ie}^* + D(s)}\Psi_C \tag{36}$$

where

$$\Psi_C = \frac{\{\phi_i^{\mathrm{T}}\}[\mathrm{M}]\{I_n\}}{m_{ie}^*} \tag{37}$$

is a constant. Then, according to Eq. (36), the performance index of H_2 optimization can be calculated as

$$J_{q_i} = \frac{1}{2\pi}\int_{-\infty}^{\infty}\left|q_i/A_g\right|^2 \mathrm{d}\lambda = \Psi_C^2\frac{1}{2\pi}\int_{-\infty}^{\infty}\left|H(\lambda)\right|^2 \mathrm{d}\lambda, \tag{38}$$

Comparing to the Eq. (12), it can be seen that Ψ_C only scales the performance index and does not affect the derivation of optimization parameters of IBDs according to the Appendix A. Therefore, the outcomes of optimization design for SDOF system can be used directly here. As a result, the optimal parameters of span-storey installed IBD or TMD can be determined by reusing the formulations in Table 1 after substituting μ by μ_{ie}.

Conclusively, when an IBD or TMD is installed on MDOF structure to suppress the response of a specific mode of vibration, the steps of design procedure are summarized as follows:

STEP 1 For the i^{th} mode of vibration, the optimum installation location is $L_{p,q}$ which have maximum of $\theta_{p,q}^{(i)} = \left(\phi_{p,i} - \phi_{q,i}\right)^2$.

STEP 2 For given inertance *b* or m_d, one can calculate μ_{ie} from Eq. (29).

STEP 3 obtain the optimal tuning ratio γ^{opt}, damping ratio ξ_d^{opt} and performance index J^{opt} from Table 1 by substituting μ with μ_{ie}.

STEP 4 The optimal stiffness and damping parameters can be obtained by

$$\left.\begin{aligned} k_d^{opt} &= b\gamma^2\omega_i^2 \\ c_d^{opt} &= 2\xi_d\sqrt{bk_d^{opt}} \end{aligned}\right\} \tag{39}$$

3.5 Case study and comparison with TMD

To comprehensively evaluate the control effect of the span-storey installation scheme, some of the benchmark structures presented in [35] are used as the primary structure hereinafter. These benchmark structures are 3-storey, 9-storey, and 20-storey steel moment-resisting frame structures designed for the SAC Phase II Steel Project and are excited by four typical actual earthquake records. The damping parameters are obtained by an assumption of Rayleigh damping. A bilinear hysteresis model is used to characterize the nonlinear behavior of these buildings when subjected to strong earthquakes. More details about these structures can be found in [35].

For parametric study and validation of the theory presented in previous sections, the simplified 3-storey benchmark structure without considering inherent damping and nonlinear behavior is used here. To evaluate the seismic control performance of span-storey installed IBDs, the complete nonlinear 9-storey benchmark structure will be used in section of earthquake response analysis.

The perimeter moment-resisting frame of the original 3-storey benchmark structure has 3-storey, 4-bay, and 20-node. Each node has three DOFs which are horizontal, vertical, and rotational. Thus the 3-storey building has 60 DOFs prior to application of boundary constraints (the detailed information can be found in MATLAB code provide by Ohtori et al. *http://sstl.cee.illinois.edu/benchmarks/*). The dimensions of the original mass and stiffness matrices are 60×60. However, in this case, only the three DOFs which present the lateral translational response of each storey are need. The static condensation method [36] is used to condense the original mass and stiffness matrices into a 3×3 matrix which only includes the three DOFs we need. The results are

$$[\mathrm{M}] = \begin{bmatrix} 478350 & 0 & 0 \\ 0 & 478350 & 0 \\ 0 & 0 & 517790 \end{bmatrix} \mathrm{kg},\ [\mathrm{K}] = \begin{bmatrix} 43.645 & -23.73 & 4.1527 \\ -23.73 & 31.342 & -12.888 \\ 4.1527 & -12.888 & 9.3407 \end{bmatrix} 10^7\ \mathrm{N/m} \tag{40}$$

The design and performance of span-storey installed IBDs and TMD are discussed. For a 3-DOF structure, there are six possible IBD installation cases, i.e., three adjacent-storey installation position $L_{0,1}$, $L_{1,2}$, $L_{2,3}$ and three span-storey installation position $L_{0,2}$, $L_{1,3}$, $L_{0,3}$. For TMD, there are only three installation cases: $L_{0,1}, L_{0,2}$ and $L_{0,3}$.

The natural modes of vibration and natural frequency of the 3-storey benchmark structure are shown in

Figure 4. Note that these agree with the results in [35].

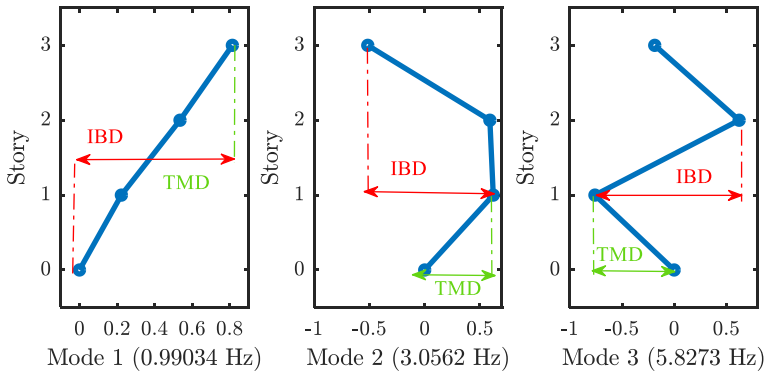

Figure 4. Lateral translational mode shapes and natural frequencies of the 3-storey benchmark structure. Red lines denote the maximal drift of modes of vibration for IBD and green lines denote that for TMD.

According to the proposed design method, the optimal $L_{p,q}$ can be determined directly by the red and green lines in

Figure 4. For example, the optimal $L_{p,q}$ for mode 2 is $L_{1,3}$ and $L_{0,1}$ for IBDs and TMD, respectively. For qualitative analysis, all AF against six position indicators are calculated.

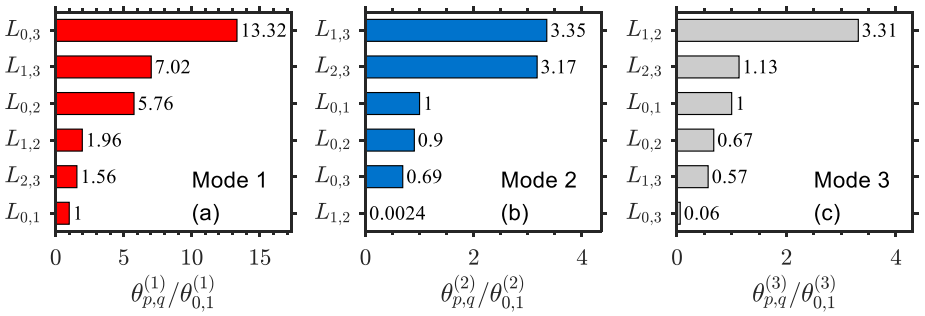

Figure 5. Comparison of AF of all position indicators for (a) mode 1; (b) mode 2; (c) mode 3.

Figure 5 shows the relative magnitude of each AF after normalized by the $\theta_{0,1}^{(i)}$. For the first modal of interest, Figure 5 (a) shows that $\theta_{0,2}^{(1)}$ and $\theta_{1,3}^{(1)}$ are greater than all adjacent installed IBDs but less than $\theta_{0,3}^{(1)}$. This indicates that the control effect of IBD on the first modal can always be improved by across more consecutive storeys. This result is obvious because the first modal is shear modal as shown in

Figure 4. For second mode, as shown in Figure 5 (b), the optimal installation position is $L_{1,3}$, followed by the adjacent installation $L_{2,3}$. Figure 5 (c) shows that the optimal installation position for the third modal control is $L_{1,2}$, which is the adjacent installation in the middle of the structure, while the span-storey installation schemes have the worst effect ($L_{0,3}$ and $L_{1,3}$).

For TMD, it can be seen that the best position for the mode 1, 2, and 3 are $L_{0,3}$, $L_{0,1}$, and $L_{0,1}$, respectively. Obviously, the IBDs outperform TMD because there are more good choices of position for IBDs. The AF ratio of IBDs and TMD when each in their best position are $\theta_{0,3}^{(1)}/\theta_{0,3}^{(1)}=1$, $\theta_{1,3}^{(2)}/\theta_{0,1}^{(2)}=3.35$ and $\theta_{1,2}^{(3)}/\theta_{0,1}^{(3)}=3.31$for mode 1, 2 and 3, respectively.

The previous works discuss the effect of installation position on the AF. Now the discussion is extended to the performance index. Defining the performance index as $J_{p,q}^{IBD-I}$ and $J_{0,q}^{TMD}$ for IBD-I and TMD, respectively. They are obtained by substituting the Eq. (29) into the expression in Table 1 and as following

$$J_{p,q}^{IBD-I}=\sqrt{\frac{4+3\mu_i\theta_{p,q}^{(i)}}{4\mu_i\theta_{p,q}^{(i)}(\mu_i\theta_{p,q}^{(i)}+1)}},\ J_{0,q}^{TMD}=\sqrt{\frac{(1+\mu_i\theta_{0,q}^{(i)})^3(1-\mu_i\theta_{0,q}^{(i)}/4)}{\mu_i\theta_{0,q}^{(i)}}} \tag{41}$$

Assuming μ_i is the same for both IBDs and TMD, then the ratio of $J_{p,q}^{IBD-I}$ to $J_{0,q}^{TMD}$ are plotted in Figure 6, where the $J_{p,q}^{IBD-I}$ considers all six positions while the $J_{0,q}^{TMD}$ only considers the best position. Figure 6 shows that all curves decreases against μ_i. This leads to IBDs mounted on inferior position can achieve the same performance with TMD mounted on superior position. For example, the $L_{1,3}$ and $L_{0,3}$ can be considered as a pair of inferior and superior positions for mode 1, and there are $J_{1,3}^{IBD-I}\approx J_{0,3}^{TMD}$ when $\mu_1=0.4$ as shown in Figure 6 (a).

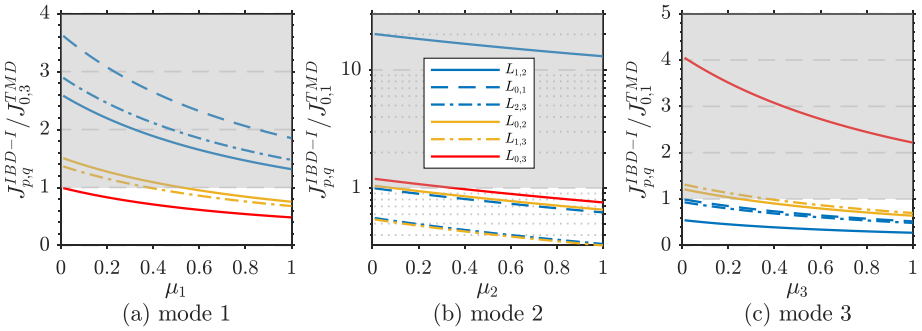

(a) mode 1 (b) mode 2 (c) mode 3

Figure 6 The comparison of performance indices of IBD-I and TMD considering $\mu_i\in[0:1]$. (a) mode 1 and the best position of TMD is $L_{0,3}$; (b) mode 2 and the best position of TMD is $L_{0,1}$; (c) mode 3 and the best position of TMD is $L_{0,1}$.

In conclusion, span-storey installation is suitable for control of low-order mode while adjacent installation is suitable for control of high-order mode. The TMD performs worse than IBDs because the fewer options for installation position and the performance decay when u_i is larger.

4. Method Validation and Parametric study

Considering all two IBDs, three modes of vibration, and six installation schemes, then there are 36 groups of optimal parameters in total to be calculated by the proposed method. Assuming the inertance b is 10% of the total mass of frame and so $b=147449\,\mathrm{kg}$, the optimal parameters of $L_{0,3}$ as example are calculated and listed in Table 2.

Table 2 The optimal parameters of IBDs for $L_{0,3}$ when targeting various modes.

	mode	μ_{ie}	γ^{opt}	k_d^{opt} (kN/m)	ξ_d^{opt}	c_d^{opt} (kNs/m)	J_{q_i} (-)
IBD-I	1	0.19389	0.87726	4396.6	0.2059	331.45	2.2244
	2	0.08022	0.94412	48463	0.13756	735.45	3.4978
	3	0.01066	0.99209	194550	0.05141	550.67	9.6748
IBD-II	1	0.19389	1	5709.1	1.1355	2083.6	2.271
	2	0.08022	1	54369	1.7654	9996.8	3.5307
	3	0.01066	1	197660	4.8438	52300	9.6876

From Table 2 it can be seen that IBD-I has better performance and smaller value of stiffness and damping in comparison to IBD-II. Then the transfer functions $q_i(j\omega)/A_g$ with optimal IBDs parameters are plotted for validation.

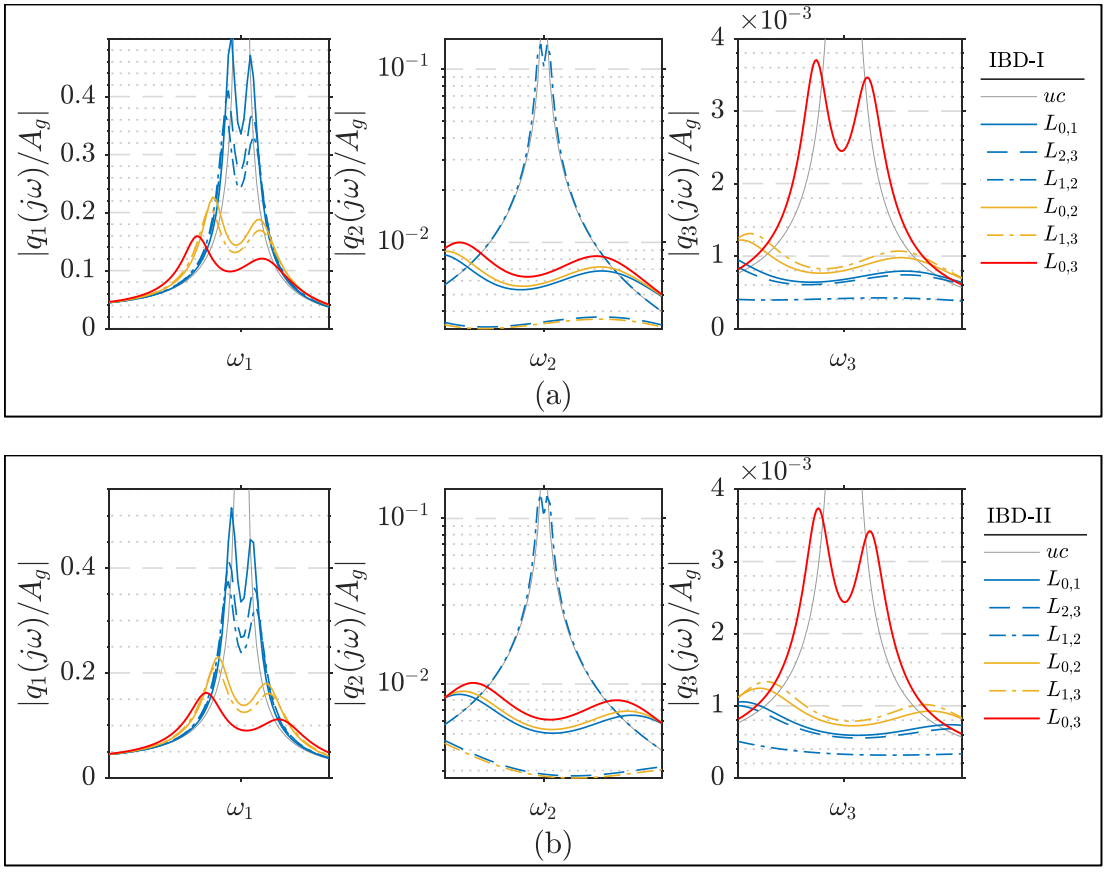

Figure 7. Frequency response curves (FRCs) of each modal coordinate response for various installation schemes: (a) IBD-I; (b) IBD-II.

The FRCs of modal response q_i of structure equipped with optimal IBD-I and IBD-II are shown in Figure 7 (a) and (b), respectively. The magnitude reduction of FRC on the natural frequency (i.e. when $\omega=\omega_1$, ω_2, or ω_3) for each installation scheme follows the same order in Figure 5, which proves the effectiveness of the $\theta_{p,q}^{(i)}$. The following sections will mainly focus on the IBD-I (TID) and response mitigation for the first modal.

4.1 Sensitivity Analysis

The optimal design of IBDs may no longer be in optimal state if structural parameters change due to damage. Therefore, it is necessary to carry out parameter sensitivity analysis. Herein, k_d and c_d is divided by its optimal value, and the ratio is restricted in limited range $k_d/k_d^{opt}\in[0.1,2]$; $c_d/c_d^{opt}\in[0.2,5]$.

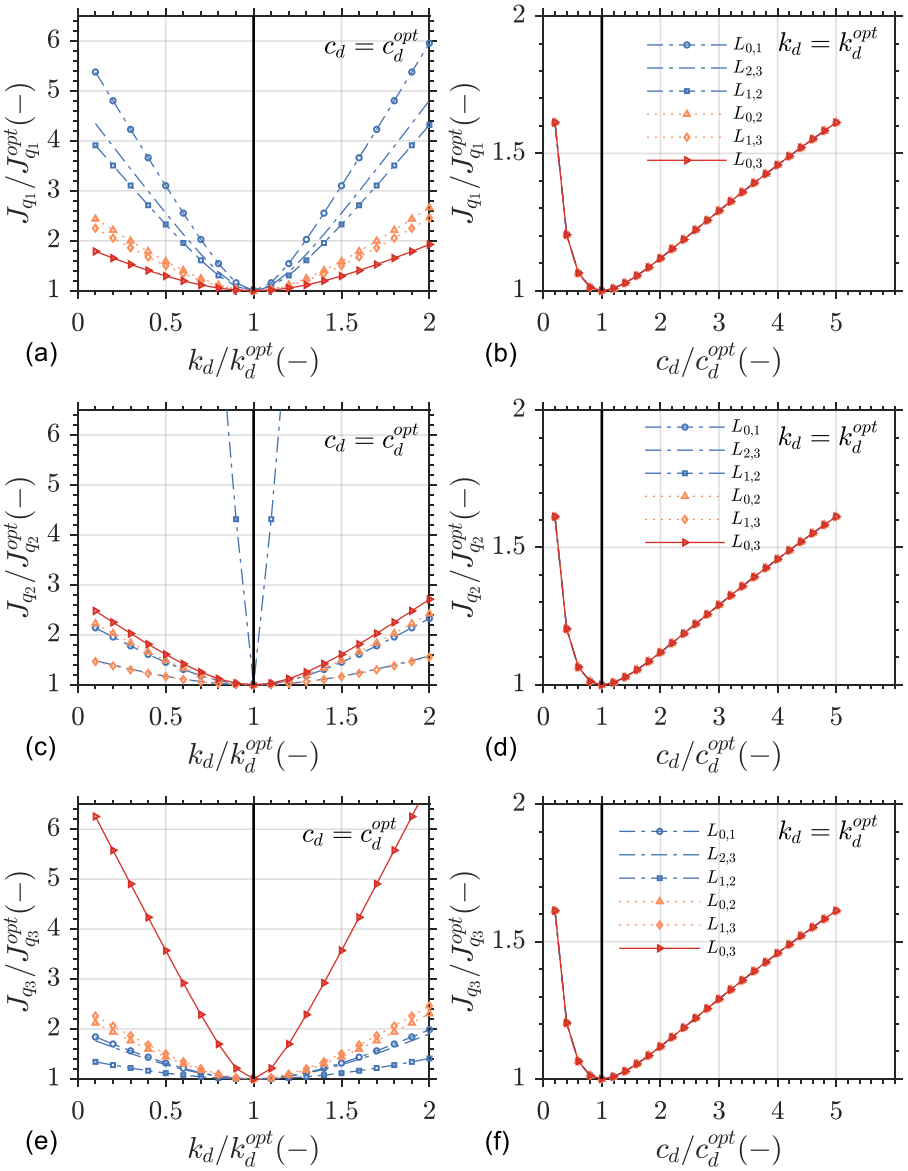

Figure 8. Sensitive analysis when IBD-I is detuned. (a) the normalized J_{q_i} against k_d/k_d^{opt} for mode 1; (b) the normalized J_{q_i} against c_d/c_d^{opt} for mode 1; (c) the normalized J_{q_i} against k_d/k_d^{opt} for mode 2; (d) the normalized J_{q_i} against c_d/c_d^{opt} for mode 2; (e) the normalized J_{q_i} against k_d/k_d^{opt} for mode 3; (f) the normalized J_{q_i} against c_d/c_d^{opt} for mode 3.

Figure 8 shows the normalized performance indices of three modes in different installation schemes when IBD-I is detuned. The sensitivity of the system performance to k_d is consistent with Figure 5 for different installation schemes, i.e., the greater the $\theta_{p,q}^{(i)}$ is, the better its robustness will be. Notably, when c_d deviates from its optimal value, the normalized performance indices of different installation schemes are almost the same, regardless what mode is considered. In conclusion, the installation placement $L_{p,q}$ which is optimal for reduction of modal response q_i also has optimal robustness when IBD is detuned.

4.2 Impulse response analysis

Impulsive load is a kind of broadband excitation and can be used to excite all modes of system to well reflect the system properties. The control effect of IBD-I due to impulse excitation will be discussed in time domain and time-frequency domain, respectively.

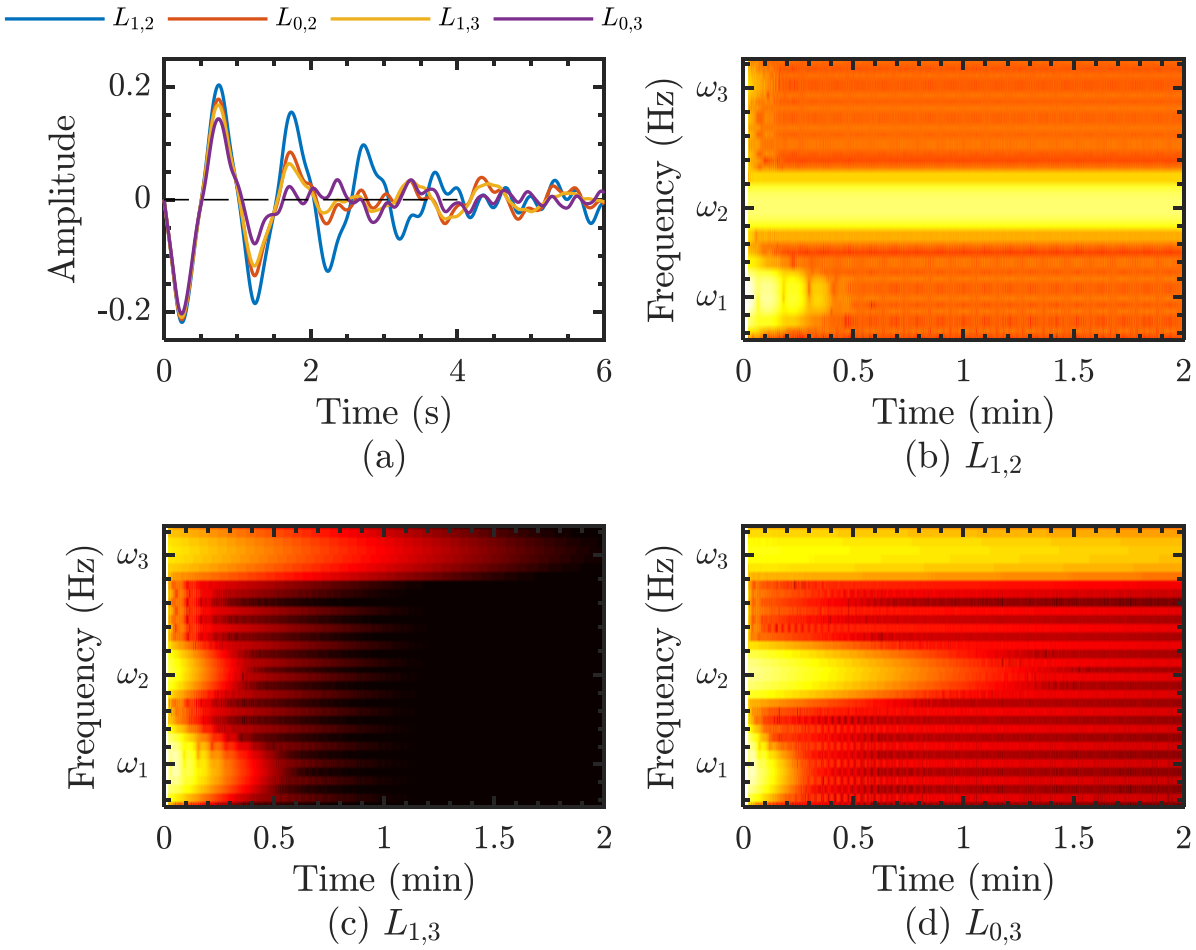

Figure 9. Displacement responses of top storey of structure due to unit impulse for IBD-I. (a) in time domain; (b)-(d) in time-frequency domain.

The impulse responses of top storey for four installation schemes are shown in Figure 9 (a). Again, the dynamic response reduction follows the same order as in Figure 5 (a), i.e., $L_{0,3}$ has the smallest peak response and the fastest attenuation rate. This is because the first modal response is primary for the 3-storey benchmark building. However, the peak time of the four curves is almost the same, which means that span-storey installation does not produce the phase change. Figure 9 (b-d) shows the time-frequency spectrum of displacements on top storey for cases $L_{1,2}$, $L_{1,3}$, and $L_{0,3}$. The attenuation rates of different modal responses vary drastically for different installation schemes. $L_{1,2}$ can basically eliminate the response of the third mode, but the attenuations of the second and first mode are somewhat invalid and inefficient, respectively. On the contrary, although $L_{0,3}$ performs worst in the case of high order mode, $L_{0,3}$ has a good attenuation rate for low order modal responses, especially has a fastest attenuation on the first modal response. $L_{1,3}$ performs excellently on attenuation of the second mode response. In general, $L_{0,3}$ has a smaller amplitude and the fastest primary modal response decay rate for civil building of which low order mode are

dominant. In conclusion, the installation placement $L_{p,q}$ which is optimal for reduction of modal response q_i also has optimal performance of attenuation for each mode response.

5. Increasing Inertance versus Span-Storey Mounting

5.1 The enhancement effect of span-storey mounting

Many studies have confirmed that increasing the inertance of IBDs system can improve the control performance. Besides, recalling the conclusion based on Eq. (32) that a larger value of $\theta_{p,q}^{(i)}$ or b will both reduce the modal response q_i, thus for first mode, adjacent-storey installed IBDs with increasing inertance (denoted as AIBDs) may have the same control performance with span-storey installed IBDs without increasing inertance (denoted as SIBDs). Here SIBDs are defined as the IBD-I installed in various span-storey positions $L_{p,q}$ and have the same inertance $b_{\text{SIBD}}=147449\,\text{kg}$. While AIBDs are considered as IBD-I installed in $L_{0,1}$ and have different inertance $b_{\text{AIBD}}=\eta\times b_{\text{SIBD}}$, where η is the inertance amplification coefficient.

According to the proposed method, AIBD and SIBD must have the same μ_{1e} if they want to have the same $J_{q_i}^{opt}$. Then η can be derived from Eq. (29) and it is

$$\eta=\frac{b_{\text{AIBD}}}{b_{\text{SIBD}}}=\frac{\theta_{p,q}^{(1)}}{\theta_{0,1}^{(1)}}=\frac{\left(\phi_{p,1}-\phi_{q,1}\right)^2}{\left(\phi_{0,1}-\phi_{1,1}\right)^2} \tag{42}$$

As a result, the amplification coefficient η can be found in Figure 5 (a). Note AIBD and SIBD also have the same γ^{opt} and ξ_d^{opt} if μ_{1e} of the both are the same, but the k_d^{opt} and c_d^{opt} are not the same according to Eq. (39). The k_d^{opt} and c_d^{opt} ratio of AIBD to SIBD is

$$\text{stiffness ratio:}\frac{b_{\text{AIBD}}\gamma^2\omega_1^2}{b_{\text{SIBD}}\gamma^2\omega_1^2}=\eta;\ \text{damping ratio:}\frac{2\xi_d\sqrt{\gamma^2\omega_1^2b^2{}_{\text{AIBD}}}}{2\xi_d\sqrt{\gamma^2\omega_1^2b^2{}_{\text{SIBD}}}}=\frac{b_{\text{AIBD}}}{b_{\text{SIBD}}}=\eta \tag{43}$$

Thus if AIBD want to have identical control performance with SIBD, one needs to magnify the inertance, damping and stiffness coefficient of AIBD according to η. In other words, η denotes the enhancement effect of SIBDs relative to AIBDs. For convenience, the AIBD which has the same performance with SIBDs installed on $L_{p,q}$ is denoted as $L_{p,q}^e$.

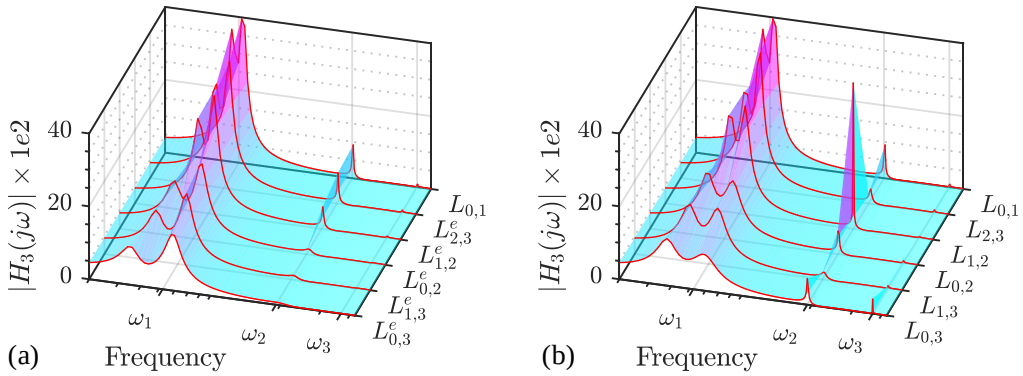

Figure 10. FRCs of top storey with (a) AIBDs with equivalent positions $L_{p,q}^e$; (b) SIBDs installed on each $L_{p,q}$.

Figure 10 shows the optimal FRCs of AIBDs and SIBSs. From Figure 10 (a), the overall FRC keeps decreasing as the increase of η, which means that increasing η of AIBD can reduce the response of all modes at the same time. While for SBIDs as shown in Figure 10 (b), Only the magnitude of FRCs of mode 1 has the same trend as AIBDs, however the other modes are not always decrease

but depend on the $\theta_{p,q}^{(i)}$. This provides more interest options, e.g. SIBD with $L_{2,3}$ and AIBD with $L_{2,3}^{e}$ have the same response on mode1 but the former have smaller response on mode 2 and larger response on mode 3.

5.2 Response analysis for harmonic excitation

This part focuses on the harmonic response analysis of AIBDs and SIBDs. Considering a sweep-frequency sine ground acceleration excitations with amplitude is $1\,\mathrm{m/s^2}$ and frequency from 0.9 Hz to 1.1 Hz which covering the first natural frequency $\omega_1 = 0.99\,\mathrm{Hz}$, the displacement and acceleration responses of top storey are plotted in Figure 11.

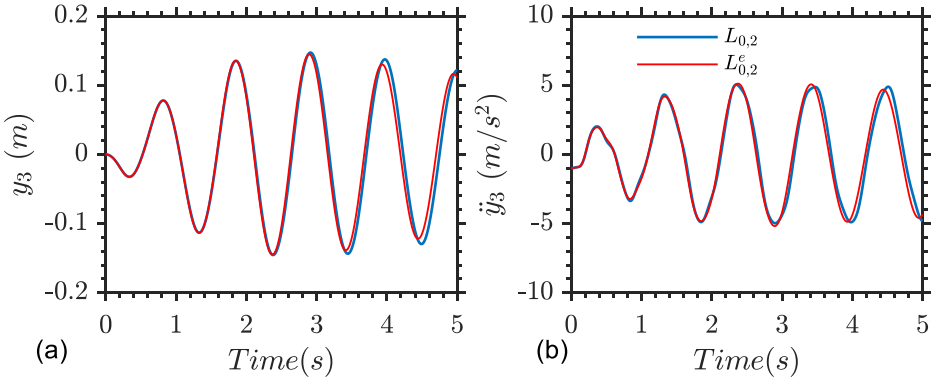

Figure 11 Harmonic responses of top storey of $L_{0,2}$ and $L_{0,2}^{e}$. (a) displacement response; (b) acceleration response.

From Figure 11 it can be seen that the AIBD with equivalent $L_{p,q}^{e}$ has quite similar control performance with that of the corresponding SIBD on displacement and acceleration responses. Then a response analysis of IBD itself is carried out below.

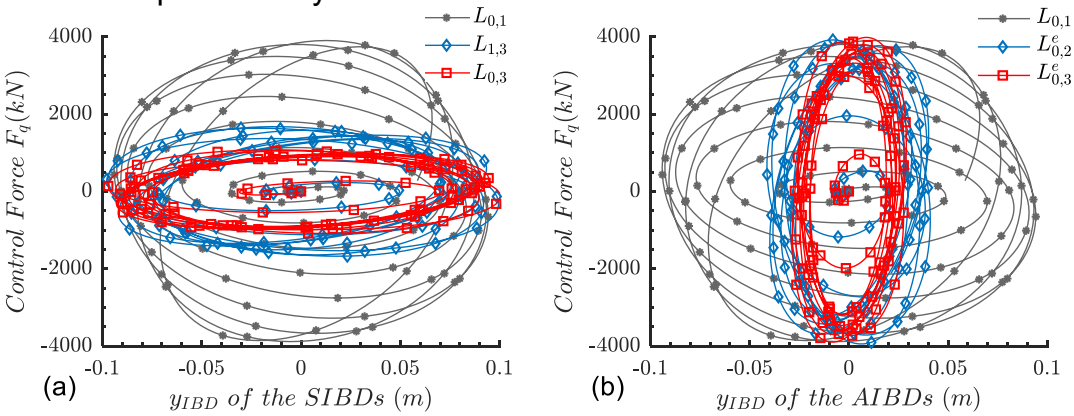

Figure 12 The hysteretic curves of (a) SIBDs installed on $L_{0,1}$, $L_{0,2}$ and $L_{0,3}$; (b) AIBDs equivalent to $L_{0,1}$, $L_{0,2}^{e}$ and $L_{0,3}^{e}$.

Figure 12 shows the hysteretic curves of SIBDs and AIBDs, in which x-axis y_{IBD} is the relative displacement between the two terminals of the IBDs and y-axis is control force F_q generated at terminals of IBDs. From Figure 12 (a), the maximum control force decreases but the maximum y_{IBD} almost unchanged when SIBDs shift from $L_{0,1}$ to $L_{0,3}$. While if AIBDs switches from $L_{0,1}$ to $L_{0,3}^{e}$, the maximum control force almost remains unchanged and the maximum y_{IBD} decrease as shown in Figure 12 (b). These results validate the conclusion in section 3.3 and indicate that the SIBDs can achieve the same performance as the AIBDs in a small peak control force through remain the maximum y_{IBD}.

6. Earthquake response analysis

6.1 Seismic control performance of the span-storey installed TID

The 9-storey nonlinear benchmark building presented in [35] and IBD-I are used for seismic response simulation. The building is 43.73m (150ft) tall and is rectangular in plan with 5 bays in both the NS and EW directions. This building model accounts for inherent damping via the Rayleigh damping formulation and material nonlinear behavior via the bilinear hysteresis model. The first three natural frequencies of the 9-storey benchmark model are 0.44Hz, 1.18Hz, and 2.05Hz, respectively.

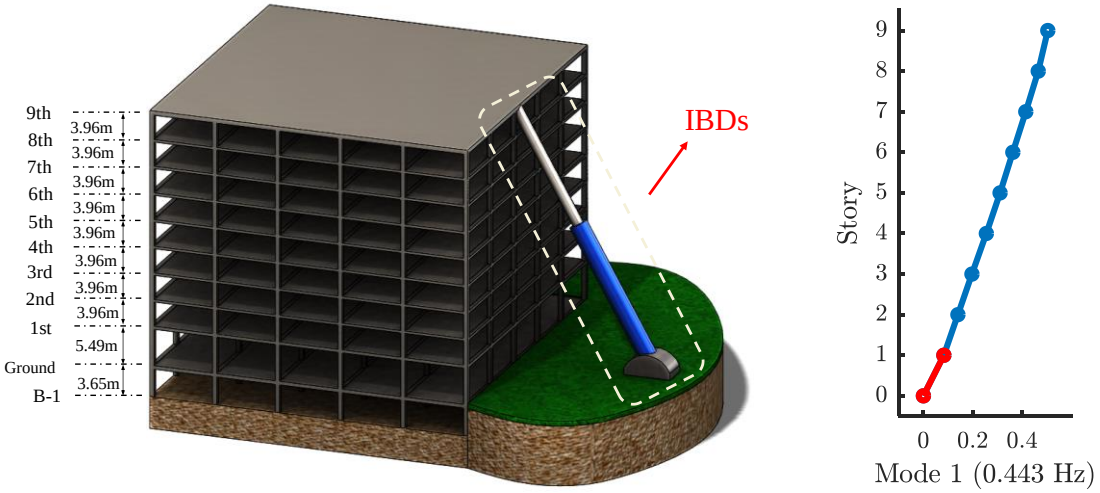

Figure 13 Conceptual illustration of the 9-storey benchmark building with a IBD (here is TID) installed between ground and top storey of building and the first mode shape of the uncontrolled building.

In seismic analysis, structural dynamic response is usually dominated by low-order modes. Previous analysis shows span-storey installation of IBDs is the best for low order modal response control. As a result, span-storey installed IBD is very suitable for structural seismic control. Herein, a span-storey and an adjacent-storey installed IBDs are considered as control device. The first mode shape of the 9-storey benchmark building is [0.0828, 0.1398, 0.1965, 0.2549, 0.3106, 0.3622, 0.4147, 0.4652, 0.5039] and is shown in Figure 13. It can be seen that the optimal installation placement are $L_{0,1}$ and $L_{0,9}$ for adjacent-storey and span-storey installed IBDs, respectively. A potential method to realize the installation of IBDs between ground and an arbitrary storey of primary structure is the outer bracing system which is also used for the MR damper [26].

The seismic mass of entire benchmark structure is about 9000 tons. The inertance of IBDs is considered as 10% of the mass. Besides, the first modal mass is determined as 504.8 tons. Then the optimal damping and stiffness parameters of IBDs can be calculated for mode 1 and the results are presented below.

Table 3 The optimal parameters of TID installed on $L_{0,1}$ and $L_{0,9}$ for first mode control of 9-storey benchmark structure

Placement	b (ton)	μ_{1e}	γ^{opt}	k_d^{opt} (kN/m)	ξ_d^{opt}	c_d^{opt} (kNs/m)
$L_{0,1}$	900	0.0122	0.99093	6839.3	0.05505	273.18
$L_{0,9}$	900	0.4527	0.76231	4047.5	0.29171	1113.5

The seismic motion data of two far-field earthquakes, (i) El Centro and (ii) Hachinohe, and two near-field earthquakes, (iii) Northridge and (iv) Kobe, are selected. In addition, various levels of each

earthquake are considered. The scale factors 0.5, 1.0, and 1.5 are applied to the El Centro and Hachinohe earthquakes and 0.5 and 1.0 are applied to the Northridge and Kobe earthquakes. Thus there have ten earthquake records are considered in the simulation. The time history of acceleration records of four earthquakes are shown in the Figure 14 (a)-(d), respectively.

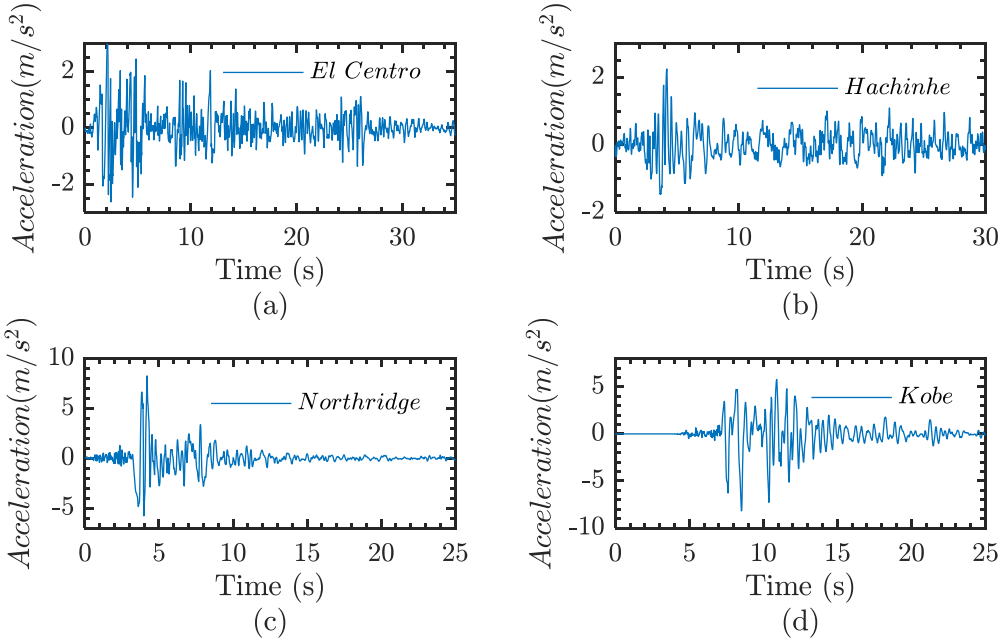

Figure 14. The earthquake acceleration data of (a) El Centro; (b) Hachinohe; (c) Northridge; (d) Kobe.

The nonlinear seismic simulator of the system show in Figure 13 base on the SIMULINK program provided by by Ohtori et al [35]. The detailed SIMULINK block diagram which simulate the nonlinear response of the span-storey installed IBD controlled benchmark structure is illustrated in Figure 15.

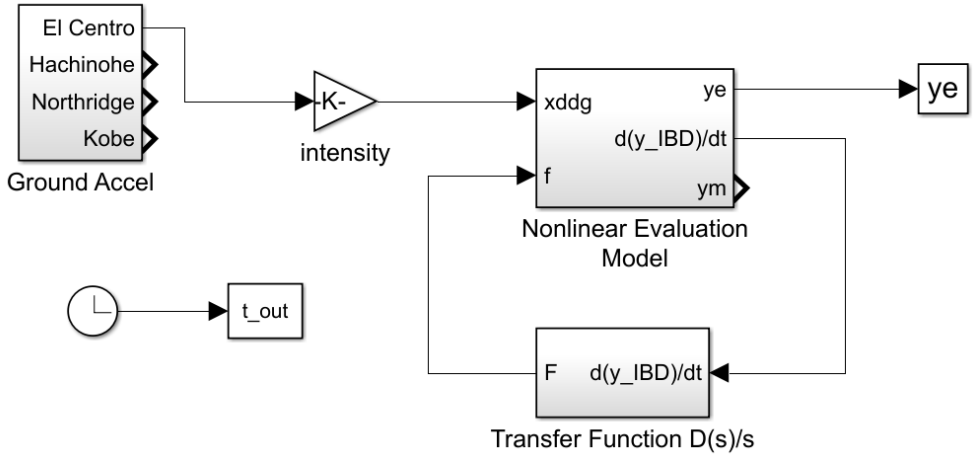

Figure 15 SIMULINK block diagram for benchmark building-IBD system simulator

The control effect of IBD is represented as the transfer function block in Figure 15. Recall that in section 2, both the control forces of IBDs can be represented in form of $|F_p| = |F_q| = D(s)Y_{IBD}$. But $D(s)$ cannot be used directly in computation of control force since the transfer function $D(s)$ is not proper (i.e., degree of denominator < degree of numerator). This can be addressed by replacing the relative displacement Y_{IBD} by relative velocity $\dot{Y}_{IBD}$ and $D(s)$ need to be modified accordingly as $D(s)/s$. Then the control forces can be calculated by the new proper transfer function $D(s)/s$, i.e., $|F_p| = |F_q| = (D(s)/s)\dot{Y}_{IBD}$. The output response $\dot{Y}_{IBD}$ can be obtained by define "*in_output_9.m*" file.

The building responses adopt peak and normed based evaluation criteria. The normed evaluation criterion is to calculate the responses by the following equation

$$\|\square\| = \sqrt{1/t_f \int_0^{t_f} [\square]^2 \, dt}$$

where t_f is the time at which response of the building is completely attenuated. The peak and norm drift ratio and absolute acceleration responses of each storey of the benchmark building subjected to 100% of El Centro earthquake record are shown in Figure 16. From Figure 16 it can be seen that the IBD with $L_{0,9}$ installation performs well in reducing all the four responses of building. The maximum response of the building with $L_{0,9}$ installation over all 9 storeys can be reduced by about 23%, 16%, 37%, and 33% in comparison to the uncontrolled building. This indicate the span-storey installation of IBDs can significantly mitigate the seismic response. While the seismic response control performance of the $L_{0,1}$ is rather insufficient. The reduction rates for $L_{0,1}$ are only 1.2%, 1.2%, 5.6%, and 4.6%, which shows no difference with uncontrolled case. Besides, both the $L_{0,9}$ and $L_{0,1}$ perform better in terms of reducing the norm and drift ratio response in comparison to the peak and acceleration response.

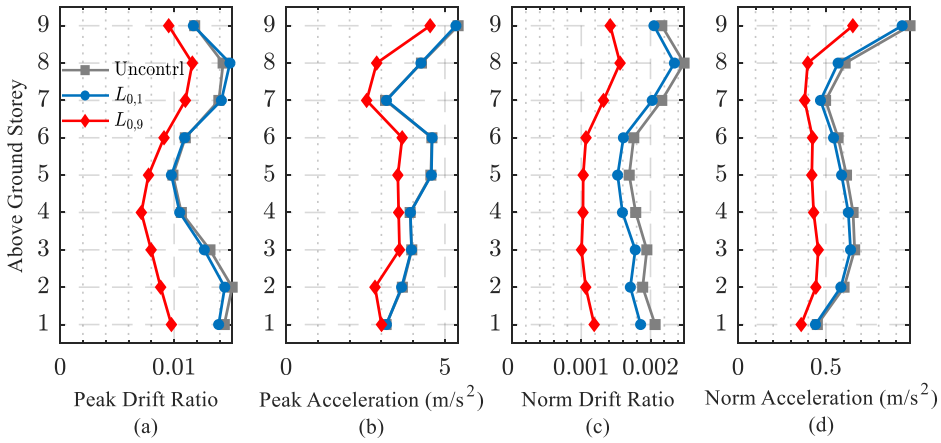

Figure 16 Responses of the IBD controlled benchmark building subjected to 100% of El Centro earthquake: (a) peak drift ratio of each storey; (b) peak acceleration of each storey; (c) norm drift ratio of each storey; (d) norm acceleration of each storey.

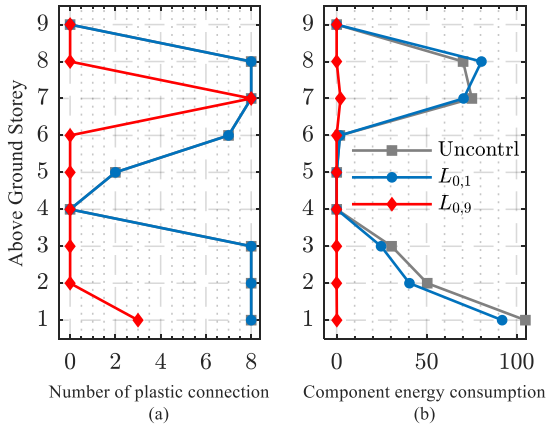

Figure 17 Building damage indexes of the IBD controlled benchmark building subjected to 100% of El Centro earthquake: (a) plastic connection number of each storey; (b) component energy consumption of each storey.

Number of plastic connection and energy consumption at the ends of the component (including beam and column) during the earthquake are the important evaluation indexes account for building

damage. Figure 17 shows the two indexes of each storey of the building subjected to 100% of El Centro earthquake. Figure 17 (a) shows that the number of plastic connection are significantly reduced from 49 to 11 when the benchmark building with $L_{0,9}$ installation. On the contrary, for the benchmark building with $L_{0,1}$ installation, the number of plastic connection remain unchanged. Figure 17 (b) shows the dissipated energy of all component ends for each storey. It can be seen that there is almost no component energy consumption when the benchmark building with $L_{0,9}$ installation relative to the uncontrolled case. For $L_{0,1}$ case, the component energy consumption at 7th storey even slight increases relative to the uncontrolled case. Figure 16 and Figure 17 indicate that the span-storey installation scheme of IBDs can effectively reduce the seismic response and significantly reduce the building damage of the 9-storey benchmark building when the El Centro earthquake is applied.

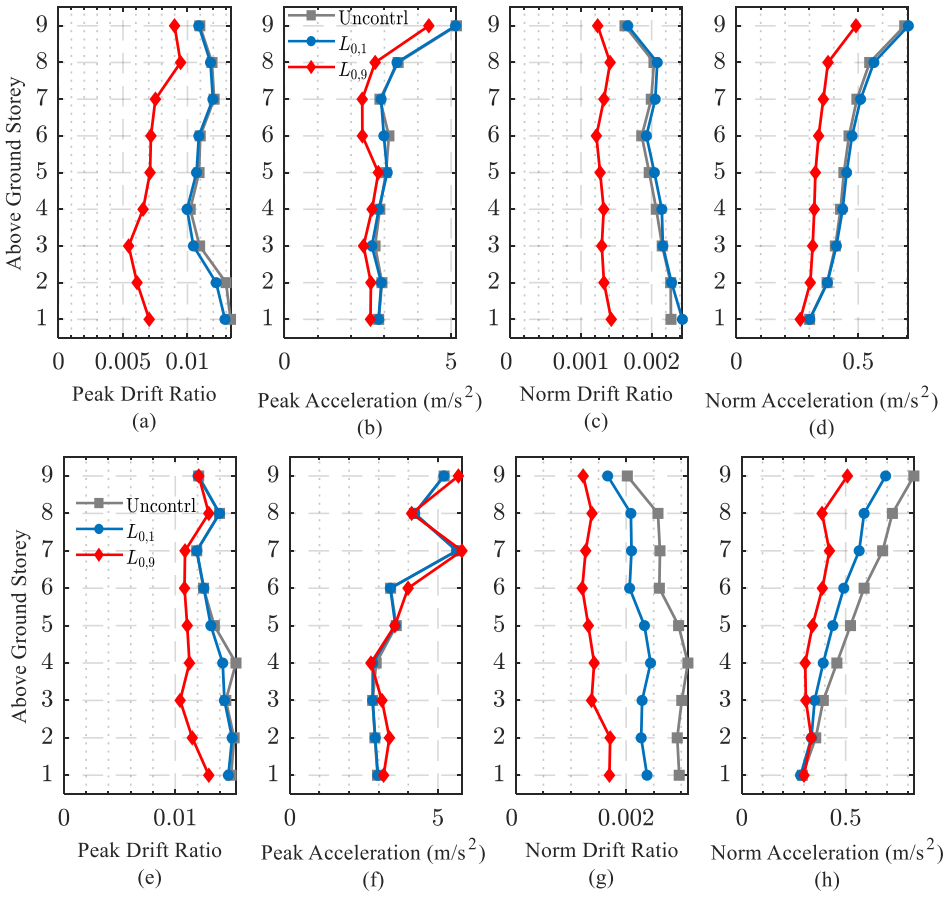

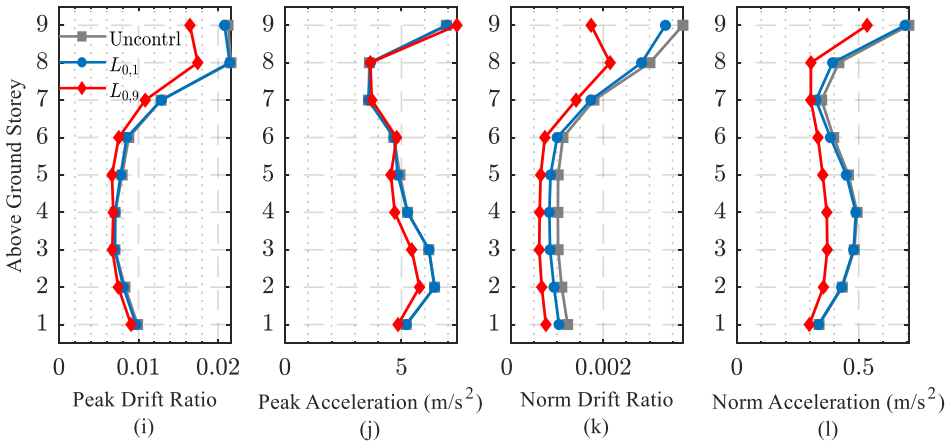

Figure 18 Responses of the IBD controlled benchmark building subjected to (a-d) 100% of Hachinohe earthquake; (e-h) 50% of Northridge earthquake; (i-l) 50% of Kobe earthquake.

The seismic responses of the benchmark building under excitations of the other three earthquake records are shown in Figure 18. The results in terms of another far-field earthquake, the Hachinohe record, are similar with previous that. However, in the case of two near-field earthquake, the control performance of $L_{0,9}$ installation is recede for peak responses, particularly for the peak acceleration response, the $L_{0,9}$ installation is almost invalid. Besides, the control performance of $L_{0,1}$ installation on norm response has improved. To comprehensively evaluate the span-storey installed IBDs system, the first ten evaluation criteria defined in the benchmark control problem [35] are adopted and the values of the evaluation criteria are provided in Table 4 of Appendix B. Please note small values of the evaluation criteria are generally more desirable.

6.2 Optimization design for the structural absolute acceleration response

From above it can be seen that the IBD perform acceptably for control of structural absolute acceleration response. This is because the design formulations in Table 1 is to minimize the performance index Eq. (10) which is the mean square value of the structural relative displacement response. In order to improve the control performance of span-storey installed IBDs for absolute acceleration response, the design formulations in [19] which aim to minimize the absolute acceleration response are used to design the IBD installed on $L_{0,9}$. The optimal parameters are $c_d = 1829.1\text{KNs/m}$ and $k_d = 5388.5\text{KN/m}$. Then the comparison of control performance between both design methods is conducted as following

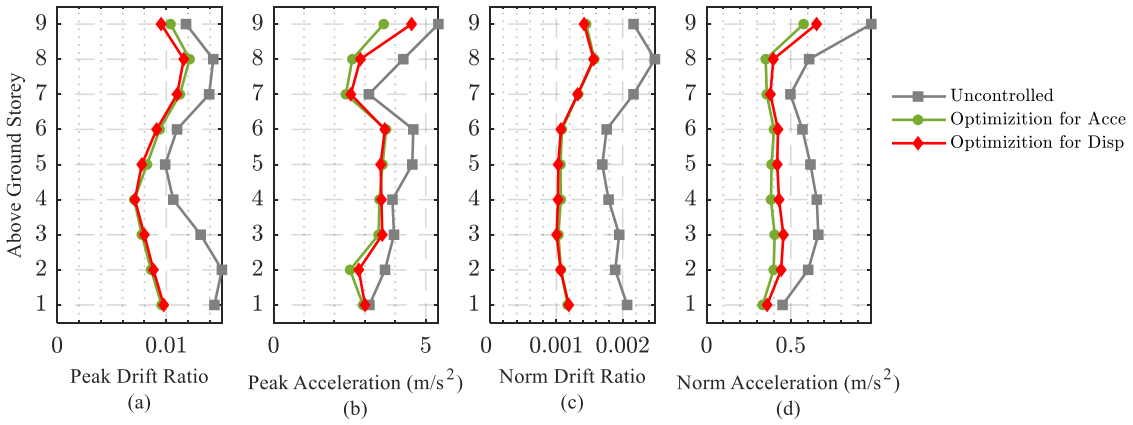

Figure 19 Structural responses of the benchmark building-IBD system subjected to 100% of El Centro earthquake, the IBD installed on $L_{0,9}$ is design respectively to reduce relative displacement and absolute acceleration response: (a) peak drift ratio of each storey; (b) peak acceleration of each storey; (c) norm drift ratio of each storey; (d) norm acceleration of each storey.

Figure 19 shows the responses of the benchmark building when the IBD is design to reduce relative displacement and absolute acceleration response according to the design formulations in Table 1 and in [19], respectively. It can be seen that the IBD optimized for acceleration performs better than the IBD optimized for displacement on control of peak and norm acceleration response of building, but performs less desirable for the control of peak and norm drift ratio relative to the other one. In practice, the design method can be chosen according to the need.

7. Conclusion

This paper provides a simplified analytical design method which can be used for two representative IBDs with span-storey mounting. A theoretical model which integrates both IBDs and TMD system is established. The influence of installation position on modal response, IBDs stroke, inerter stroke, and control force produced by IBDs are analytically investigated. A 3-storey benchmark building model is introduced for case study and the comparative study on the span-storey installed IBDs and the TMD is carried out. The sensitivity analysis and impulse response analysis are proposed for parametric study and validating the analytical design method. A comparison of the span-storey mounting with increasing inertance is examined. In the end the seismic control performance of span-storey installed IBDs on 9-storey nonlinear benchmark building is evaluated.
The principal outcomes of this research are summarized as follows: (i) an analytical design method of span-storey installed IBDs is developed and it is convenient and effective through reusing the design formulas in SDOF case. Besides, the influence of the installation position of IBDs on each modal response, IBDs stroke, inerter stroke, and control force produced by IBDs is derived and this can be used to determine the installation position of IBDs; (ii) the span-storey installation and the adjacent-storey installation of IBDs have excellent performance of control and robustness for lower order and higher order mode, respectively. The span-storey installation have excellent attenuation rate for first mode and does not produce the phase change; (iii) the span-storey installed IBDs outperform the TMD while dealing with dynamic loadings since the former have more options for installation positions and the performance of IBDs will not decay like that of TMD when μ is larger.; and (iv) Through comparing SIBDs and AIBDs, the span-storey installation can substantially improve the efficiency of inerter and damper and reduce the control force by amplifying the drift has been confirmed since the SIBDs with small inertance, damping coefficient and control force can achieve the same performance with AIBDs; (v)Finally, a 9-storey seismically excited nonlinear benchmark building is used to evaluate the control performance of the IBDs. The results show that the span-storey installed IBDs has a high efficiency in seismic control and can significant reduce the building damage.

Declaration of Competing Interest

The authors declared that they have no conflicts of interest to this work.

Appendix A

According to Asami [37], the optimal parameters can be found by the solution of partial differential equations:

$$\left.\begin{aligned}\frac{\partial J}{\partial \gamma}=0\\ \frac{\partial J}{\partial \xi_d}=0\end{aligned}\right\} \tag{A.1}$$

According to Hu [16], the $H(s)$ of IBD-I is identical to that of a SDOF structure-TMD system when excitation is external force. Thus the optimal parameters of IBD-I can be found by the previous studies of TMD derived by Warburton [33].

For IBD-II, when $\xi_s=0$ the performance index J is

$$J=\frac{\xi_d^2(4\gamma^4\mu-8\gamma^2+4\gamma^4+4)+\gamma^2}{4\xi_d\gamma^3\mu} \tag{A.2}$$

Then the Eq. (A.1) can be given by

$$\left.\begin{aligned}4\xi_d^2-\gamma^2-8\xi_d^2\gamma^2+4\xi_d^2\gamma^4+4\xi_d^2\gamma^4\mu=0\\ 8\xi_d^2\gamma^2-\gamma^2-12\xi_d^2+4\xi_d^2\gamma^4+4\xi_d^2\gamma^4\mu=0\end{aligned}\right\} \tag{A.3}$$

The solutions of Eq. (A.3), i.e. the optimal parameters of IBD-II, are

$$\left.\begin{aligned}\gamma^{opt}=1\\ \xi_d^{opt}=\frac{1}{2\sqrt{\mu}}\end{aligned}\right\} \tag{A.4}$$

Finally, the optimal performance index can be obtained by substituting Eq. (A.4) into (A.2):

$$J^{opt}=\frac{1}{\sqrt{\mu}} \tag{A.5}$$

Appendix B

Table 4 Earthquake evaluation criteria for the IBD-I installed at $L_{0.9}$

Earthquake (intensity)	**El Centro (0.5/1.0/1.5)**	**Hachinohe (0.5/1.0/1.5)**	**Northridge (0.5/1.0)**	**Kobe (0.5/1.0)**
Peak Drift Ratio	0.67625 0.76853 0.76501	0.67646 0.70985 0.75551	0.84211 0.94721	0.80674 0.88505
Peak Level Accel.	0.69040 0.83746 0.95868	0.83561 0.83931 0.98159	1.03145 1.09689	1.06565 0.98603
Peak Base Shear	0.65146 0.86991 0.96609	0.57493 0.68659 0.92535	0.94715 1.09114	0.96125 0.93214
Norm Drift Ratio	0.51754 0.62788 0.87059	0.60747 0.62830 0.59418	0.54827 0.65960	0.57698 0.64749
Norm Level Accel.	0.56653 0.66758 0.71850	0.65178 0.71064 0.80034	0.61389 0.76498	0.75743 0.88672
Norm Base Shear	0.48772	0.63535	0.50615	0.66240

	0.62696 0.73701	0.67718 0.74598	0.67990	0.87461
Ductility	0.63992 0.55714 0.64765	0.58785 0.47189 0.70999	0.77854 0.99923	0.77467 0.90758
Dissipated Energy	-- 0.06169 0.43162	-- 0.00000 0.21622	0.21212 0.51267	0.41133 0.76680
Plastic Connections	-- 0.22449 0.79710	-- 0.00000 0.47887	0.88889 1.05333	0.92308 0.94737
Norm Ductility	0.51188 0.51798 0.97126	0.60585 0.51187 0.44327	1.03735 0.76127	0.70639 0.54605

References

1. Smith MC. Synthesis of mechanical networks: The inerter【J】. *IEEE Transactions on Automatic Control* 2002; **47**(10): 1648–1662. DOI: 10.1109/TAC.2002.803532.
2. Ikago K, Sugimura Y, Saito K, Inoue N. Seismic displacement control of multiple-degree-of-freedom structures using tuned viscous mass dampers. *Proceedings of the 8th International Conference on Structural Dynamics, EURODYN 2011* 2011; **1**(3): 1800–1807.
3. Kohju Ikago KS and NI. Seismic control of single-degree-of-freedom structure using tuned viscous mass damper. *Earthquake Engineering and Structural Dynamics* 2012; **41**(3): 453–474. DOI: 10.1002/eqe.
4. Marian L, Giaralis A. Optimal design of a novel tuned mass-damper-inerter (TMDI) passive vibration control configuration for stochastically support-excited structural systems. *Probabilistic Engineering Mechanics* 2014; **38**: 156–164. DOI: 10.1016/j.probengmech.2014.03.007.
5. Pietrosanti D, De Angelis M, Basili M. Optimal design and performance evaluation of systems with Tuned Mass Damper Inerter (TMDI). *Earthquake Engineering and Structural Dynamics* 2017; **46**(8): 1367–1388. DOI: 10.1002/eqe.2861.
6. De Domenico D, Ricciardi G. An enhanced base isolation system equipped with optimal tuned mass damper inerter (TMDI). *Earthquake Engineering and Structural Dynamics* 2018; **47**(5): 1169–1192. DOI: 10.1002/eqe.3011.
7. De Domenico D, Ricciardi G. Optimal design and seismic performance of tuned mass damper inerter (TMDI) for structures with nonlinear base isolation systems. *Earthquake Engineering and Structural Dynamics* 2018; **47**(12): 2539–2560. DOI: 10.1002/eqe.3098.
8. Di Matteo A, Masnata C, Pirrotta A. Simplified analytical solution for the optimal design of Tuned Mass Damper Inerter for base isolated structures. *Mechanical Systems and Signal Processing* 2019; **134**: 106337. DOI: 10.1016/j.ymssp.2019.106337.
9. De Angelis M, Giaralis A, Petrini F, Pietrosanti D. Optimal tuning and assessment of inertial dampers with grounded inerter for vibration control of seismically excited base-isolated systems. *Engineering Structures* 2019; **196**(November 2018): 109250. DOI: 10.1016/j.engstruct.2019.05.091.
10. Xu K, Bi K, Han Q, Li X, Du X. Using tuned mass damper inerter to mitigate vortex-induced vibration of long-span bridges: Analytical study. *Engineering Structures* 2019; **182**(November 2018): 101–111. DOI: 10.1016/j.engstruct.2018.12.067.
11. I.F.Lazar, Neild SA, Wagg DJ. Using an inerter-based device for structural vibration suppression. *Earthquake Engineering and Structural Dynamics* 2014; **43**(8): 1129–1147.

12. Lazar IF, Neild SA, Wagg DJ. Performance analysis of cables with attached tuned-inerter-dampers. *Conference Proceedings of the Society for Experimental Mechanics Series* 2015; **2**: 433–441. DOI: 10.1007/978-3-319-15248-6_44.
13. Lazar IF, Neild SA, Wagg DJ. Vibration suppression of cables using tuned inerter dampers. *Engineering Structures* 2016; **122**: 62–71. DOI: 10.1016/j.engstruct.2016.04.017.
14. Sun L, Hong D, Chen L. Cables interconnected with tuned inerter damper for vibration mitigation. *Engineering Structures* 2017; **151**: 57–67. DOI: 10.1016/j.engstruct.2017.08.009.
15. Radu A, Lazar IF, Neild SA, Sextos A. Risk assessment of cables vibration-suppressed with tuned-inerter dampers. *Engineering Structures* 2020; **222**(June): 111127. DOI: 10.1016/j.engstruct.2020.111127.
16. Hu Y, Chen MZQ, Shu Z, Huang L. Analysis and optimisation for inerter-based isolators via fixed-point theory and algebraic solution. *Journal of Sound and Vibration* 2015; **346**(1): 17–36. DOI: 10.1016/j.jsv.2015.02.041.
17. Hu Y, Chen MZQ. Performance evaluation for inerter-based dynamic vibration absorbers. *International Journal of Mechanical Sciences* 2015; **99**: 297–307. DOI: 10.1016/j.ijmecsci.2015.06.003.
18. Wen Y, Chen Z, Hua X. Design and Evaluation of Tuned Inerter-Based Dampers for the Seismic Control of MDOF Structures. *Journal of Structural Engineering (United States)* 2017; **143**(4): 1–11. DOI: 10.1061/(ASCE)ST.1943-541X.0001680.
19. Xu T, Li Y, Lai T, Zheng J. A simplified design method of tuned inerter damper for damped civil structures: Theory, validation, and application. *Structural Control and Health Monitoring* 2021(January): e2789. DOI: 10.1002/stc.2798.
20. Pan C, Zhang R. Design of structure with inerter system based on stochastic response mitigation ratio. *Structural Control and Health Monitoring* 2018; **25**(6): 1–21. DOI: 10.1002/stc.2169.
21. Shen W, Niyitangamahoro A, Feng Z, Zhu H. Tuned inerter dampers for civil structures subjected to earthquake ground motions: optimum design and seismic performance. *Engineering Structures* 2019; **198**: 109470. DOI: 10.1016/j.engstruct.2019.109470.
22. Lazar IF, Radu A. Reliability of Vibration- Suppressed Structures Under Seismic Loads. *11th US National Conference on Earthquake Engineering* 2018.
23. Radu A, Lazar IF. Reliability of controlled linear systems under Gaussian and non-Gaussian loads. *International Journal of Dynamics and Control* 2019; **7**(4): 1489–1500. DOI: 10.1007/s40435-019-00562-5.
24. Zhang R, Zhao Z, Pan C, Ikago K, Xue S. Damping enhancement principle of inerter system. *Structural Control and Health Monitoring* 2020. DOI: 10.1002/stc.2523.
25. Deastra P, Wagg D, Sims N, Akbar M. Tuned inerter dampers with linear hysteretic damping. *Earthquake Engineering and Structural Dynamics* 2020; **49**(12): 1216–1235. DOI: 10.1002/eqe.3287.
26. Aly AM. The Use of Bracing Systems with MR Dampers in Super Tall Buildings. *International Journal of High-Rise Buildings* 2016; **5**(1): 31–41. DOI: 10.21022/ijhrb.2016.5.1.31.
27. Constantinou MC, Soong TT, Dargush GF. TOGGLE-BRACE-DAMPER SEISMIC ENERGY DISSIPATION SYSTEMS. *Journal of Structural Engineering* 2001; **9445**(February). DOI: 10.1061/(ASCE)0733-9445(2001)127.
28. Hwang J seung, Kim J, Kim Y moon. Rotational inertia dampers with toggle bracing for vibration control of a building structure. *Engineering Structures* 2007; **29**: 1201–1208. DOI: 10.1016/j.engstruct.2006.08.005.
29. Giaralis A, Petrini F. Wind-Induced Vibration Mitigation in Tall Buildings Using the Tuned Mass-Damper-Inerter. *Journal of Structural Engineering (United States)* 2017; **143**(9): 1–11. DOI: 10.1061/(ASCE)ST.1943-541X.0001863.

30. Giaralis A, Taflanidis AA. Optimal tuned mass-damper-inerter (TMDI) design for seismically excited MDOF structures with model uncertainties based on reliability criteria. *Structural Control and Health Monitoring* 2018; **25**(2): 1–22. DOI: 10.1002/stc.2082.
31. Xue S, Kang J, Xie L, Zhang R, Ban X. Cross-Layer installed cable-bracing inerter system for MDOF structure seismic response control. *Applied Sciences (Switzerland)* 2020; **10**(17). DOI: 10.3390/app10175914.
32. Asami T, Nishihara O, Baz AM. Analytical solutions to H∞ and H 2 optimization of dynamic vibration absorbers attached to damped linear systems. *Journal of Vibration and Acoustics* 2002; **124**(2): 284–295. DOI: 10.1115/1.1456458.
33. Warburton GB. Optimum absorber parameters for various combinations of response and excitation parameters. *Earthquake Engineering & Structural Dynamics* 1982; **10**(3): 381–401. DOI: 10.1002/eqe.4290100304.
34. Rana R, Soong TT. Parametric study and simplified design of tuned mass dampers. *Engineering Structures* 1998; **20**(3): 193–204. DOI: 10.1016/S0141-0296(97)00078-3.
35. Ohtori Y, Christenson RE, Spencer BF, Dyke SJ. Benchmark control problems for seismically excited nonlinear buildings. *Journal of Engineering Mechanics* 2004; **130**(4): 366–385. DOI: 10.1061/(ASCE)0733-9399(2004)130:4(366).
36. Anil K.Chopra. *DYNAMICS OF STRUCTURES Theory and Applications to Earthquake Engineering*. 2013. DOI: 10.1002/9781118599792.
37. Asami T. Optimum Design of Dynamic Absorbers for a System Subjected to Random Excitation*. *JSME International Journal* 1991; **34**(2): 218–226.